J Physiol 586.23 (2008) pp 5679–5700

The Journal of Physiology

Autonomous initiation and propagation of action potentials in neurons of the subthalamic nucleus

Jeremy F. Atherton, David L. Wokosin, Sankari Ramanathan and Mark D. Bevan

Department of Physiology, Feinberg School of Medicine, Northwestern University, 303 E. Chicago Avenue, Chicago, IL 60611, USA

The activity of the subthalamic nucleus (STN) is intimately related to movement and is generated, in part, by voltage-dependent Na^+ (Na_v) channels that drive autonomous firing. In order to determine the principles underlying the initiation and propagation of action potentials in STN neurons, 2-photon laser scanning microscopy was used to guide tight-seal whole-cell somatic and loose-seal cell-attached axonal/dendritic patch-clamp recordings and compartment-selective ion channel manipulation in rat brain slices. Action potentials were first detected in a region that corresponded most closely to the unmyelinated axon initial segment, as defined by Golgi and ankyrin G labelling. Following initiation, action potentials propagated reliably into axonal and somatodendritic compartments with conduction velocities of ~5 m s^{-1} and ~0.7 m s^{-1}, respectively. Action potentials generated by neurons with axons truncated within or beyond the axon initial segment were not significantly different. However, axon initial segment and somatic but not dendritic or more distal axonal application of low [Na^+] ACSF or the selective Na_v channel blocker tetrodotoxin consistently depolarized action potential threshold. Finally, somatodendritic but not axonal application of GABA evoked large, rapid inhibitory currents in concordance with electron microscopic analyses, which revealed that the somatodendritic compartment was the principal target of putative inhibitory inputs. Together the data are consistent with the conclusions that in STN neurons the axon initial segment and soma express an excess of Na_v channels for the generation of autonomous activity, while synaptic activation of somatodendritic $GABA_A$ receptors regulates the axonal initiation of action potentials.

(Received 25 April 2008; accepted after revision 29 September 2008; first published online 2 October 2008)
Corresponding author M. D. Bevan: Department of Physiology, Feinberg School of Medicine, Northwestern University, 303 E. Chicago Avenue, Chicago, IL 60611, USA. Email: m-bevan@northwestern.edu

The glutamatergic subthalamic nucleus (STN) is a key component of the basal ganglia, a group of subcortical brain nuclei that are critical for normal voluntary movement (DeLong *et al.* 1986; Graybiel *et al.* 1994; Bar-Gad *et al.* 2003; Hikosaka *et al.* 2006). The activity of the STN has a complex relationship to movement but appears important for the suppression of ill-timed/inappropriate muscle contractions (Albin *et al.* 1989; Crossman, 1989; DeLong, 1990; Mink & Thach, 1993). Indeed, pathological/experimental ablation of the STN leads to ballistic/choreic movement (Albin *et al.* 1989; Crossman, 1989; DeLong, 1990; Mink & Thach, 1993), whereas pathological overactivity and correlated burst firing in the STN are associated with akinesia, rigidity and tremor in Parkinson's disease (PD) (Albin *et al.* 1989; Crossman, 1989; DeLong, 1990; Mink & Thach, 1993; Bergman *et al.* 1994; Levy *et al.* 2000, 2002). The role of the STN is further evidenced by the fact that correction of its pathological activity, by direct high-frequency electrical stimulation, ablation or drug treatment, profoundly ameliorates the motor symptoms of PD (Bergman *et al.* 1990; Brown *et al.* 2001; Levy *et al.* 2001; Benabid, 2003; Alvarez *et al.* 2005; Hamani *et al.* 2006).

In recent years, it has been shown that STN neurons fire rhythmically and independently of synaptic input (Bevan & Wilson, 1999; Beurrier *et al.* 2000; Do & Bean, 2003; Baufreton *et al.* 2005). This autonomous firing may contribute to the tonic discharge of STN neurons *in vivo* and influence synaptic integration. Autonomous firing is generated by voltage-dependent Na^+ (Na_v) channels that underlie persistent, transient and resurgent currents (Bevan & Wilson, 1999; Beurrier *et al.* 2000; Do & Bean, 2003; Baufreton *et al.* 2005). The location of Na_v channels and the manner in which action potentials are initiated and propagated in STN neurons are, however, less well defined. In the few neurons studied thus far, autonomously/synaptically generated action potentials are usually initiated in regions of myelinated

This paper has online Supplemental material.

DOI: 10.1113/jphysiol.2008.155861

or non-myelinated axons proximal to the soma (Clark *et al.* 2005; Palmer & Stuart, 2006; Kole *et al.* 2007, 2008; Meeks & Mennerick, 2007; Shu *et al.* 2007; Schmidt-Hieber *et al.* 2008). In myelinated axons initiation is at the initial segment or at the first node of Ranvier (Clark *et al.* 2005; Palmer & Stuart, 2006; Kole *et al.* 2007, 2008; Meeks & Mennerick, 2007; Scott *et al.* 2007; Shu *et al.* 2007; Schmidt-Hieber *et al.* 2008). The proximal axon is also the strongest site of Na_v channel expression as evidenced by immunocytochemical labelling and patch clamp recording (Astman *et al.* 2006; Kuba *et al.* 2006; Castelli *et al.* 2007; Meeks & Mennerick, 2007; Scott *et al.* 2007; Van Wart *et al.* 2007; Kole *et al.* 2008). It has also been suggested that Na_v channels are distributed similarly across neurons but axonal channels possess a lower activation voltage (Colbert & Pan, 2002) and thus lead action potential generation. Theoretical studies support the view that high Na_v channel density and/or a lower activation voltage together with a low effective capacitance favour the initiation of action potentials in the proximal axon (Mainen *et al.* 1995; Colbert & Pan, 2002; Clark *et al.* 2005; Mercer *et al.* 2007; Kole *et al.* 2008; Schmidt-Hieber *et al.* 2008). Our *first objective* was therefore to determine the site of autonomous action potential initiation in STN neurons. Because direct recordings from most compartments of small neurons like STN neurons are difficult due to their poor visibility and fine calibre, STN neurons were filled with a fluorescent marker via a somatic patch-clamp electrode in the whole-cell configuration and then imaged using 2-photon laser scanning microscopy (2PLSM) (Clark *et al.* 2005; Khaliq & Raman, 2005; Meeks *et al.* 2005; Monsivais *et al.* 2005; Schmidt-Hieber *et al.* 2008). Visually guided loose-seal cell-attached recordings of axonal and dendritic action potentials were then acquired and compared to somatic records to determine the earliest site of action potential generation.

Armed with an appreciation of the initiation region, our *second objective* was to determine the morphological properties of the proximal STN axon. Thus, the Golgi technique, due to its relative efficiency of labelling non-myelinated compartments (Fairen *et al.* 1977; Afsharpour, 1985; Peters, 2007), was employed to estimate the length of the axon initial segment and ankyrin G labelling was used to determine the location of the first node of Ranvier (Bennett & Lambert, 1999).

The ortho- and antidromic propagation of action potentials from the site of initiation can be faithful or exhibit failures and/or attenuation (Coombs *et al.* 1957; Fuortes *et al.* 1957; Grossman *et al.* 1979; Grace & Bunney, 1983; Spruston *et al.* 1995; Debanne *et al.* 1997, 2004; Jung *et al.* 1997; Khaliq & Raman, 2005; Monsivais *et al.* 2005; Gentet & Williams, 2007; Shu *et al.* 2007). Failure/attenuation can be due to a low density or relative susceptibility to inactivation of Na_v channels and/or placement of other channels that limit Na_v channel activation (Debanne *et al.* 1997, 2004; Jung *et al.* 1997; Gentet & Williams, 2007; Kole *et al.* 2007, 2008; Scott *et al.* 2007). Failure may also be due to the higher capacitance of branch points (Grossman *et al.* 1979; Debanne, 2004). Our *third objective* was therefore to determine whether autonomously generated action potentials propagate reliably in STN neurons.

Despite the importance of axonal Na_v channels, acutely isolated STN and cerebellar Purkinje neurons retain autonomous activity and large Na_v channel currents despite truncation of the axon to $< 10\,\mu$m (Raman & Bean, 1999; Do & Bean, 2003; Baufreton *et al.* 2005). These data suggest that somatodendritic Na_v channels also contribute to firing. Our *fourth objective* was therefore to determine the relative contribution of each neuronal compartment to autonomous firing. The first approach compared the firing of neurons whose axons were variably truncated; the second approach utilized compartment-selective reduction in Na_v channel current by local application of media containing a low $[Na^+]$ or tetrodotoxin (TTX).

In many neurons axosomatic and axoaxonic GABAergic synapses close to/at the site of initiation tightly regulate firing (Buhl *et al.* 1995; Miles *et al.* 1996; Häusser & Clark, 1997; Pouzat & Hestrin, 1997; Person & Perkel, 2005; Szabadics *et al.* 2006). In STN neurons, the available evidence suggests that GABAergic synaptic inputs are directed to the axon hillock and somatic and dendritic compartments (Chang *et al.* 1983; Smith *et al.* 1990; Shink *et al.* 1996; Bevan *et al.* 1997) where they profoundly influence autonomous firing (Bevan *et al.* 2002; Baufreton *et al.* 2005). Our *final objective* was therefore to determine the precise location of GABAergic inputs relative to the initiation site, through ultrastructural analysis of Golgi-labelled neurons and compartment-selective application of GABA.

Methods

Ethical information

All procedures involving animals were carried out in accordance with Northwestern University's Institutional Animal Care and Use Committee and the policies of the National Institutes of Health (USA).

Slice preparation

Brain slices were prepared from 60 male 16- to 25-day-old Sprague–Dawley rats (Charles River, Wilmington, MA, USA), as previously described. Rats were deeply anaesthetized with ketamine/xylazine ($87/13\,mg\,kg^{-1}$ I.P.) before transcardial perfusion with ~25 ml of ice-cold modified artificial cerebrospinal fluid (ACSF) that contained 230 mM sucrose, 2.5 mM KCl,

1.25 mM $NaH_2PO_4.H_2O$, 0.5 mM $CaCl_2.2H_2O$, 10 mM $MgSO_4.7H_2O$, 10 mM glucose and 26 mM $NaHCO_3$ (equilibrated with 95% O_2 and 5% CO_2). Each brain was then removed, immersed in modified ACSF and sectioned at 300 μm in the sagittal, coronal or horizontal planes (3000 Deluxe, Vibratome Company, St Louis, MO, USA). Slices containing the STN were then transferred to a holding chamber where they were submerged in traditional ACSF containing 125 mM NaCl, 2.5 mM KCl, 1.25 mM $NaH_2PO_4.H_2O$, 2 mM $CaCl_2.2H_2O$, 2 mM $MgSO_4.7H_2O$, 10 mM glucose, and 26 mM $NaHCO_3$ (equilibrated with 95% O_2 and 5% CO_2) and maintained at room temperature.

Electrophysiology and 2PLSM

Individual brain slices were transferred to a recording chamber that was perfused at 2–3 ml min^{-1} with media that more closely matched rodent brain interstitial fluid (Sanchez-Vives & McCormick, 2000). Thus, 'synthetic interstitial fluid' contained 126 mM NaCl, 3 mM KCl, 1.25 mM $NaH_2PO_4.H_2O$, 1.6 mM $CaCl_2.2H_2O$, 1.5 mM $MgSO_4.7H_2O$, 10 mM glucose, and 26 mM $NaHCO_3$ (equilibrated with 95% O_2 and 5% CO_2) and was heated to 35–37°C. Electrophysiological recordings employed borosilicate glass micropipettes (Warner Instruments, Hamden, CT, USA) prepared with a micropipette puller (P97, Sutter Instruments, Novato, CA, USA). Pipettes had an impedance of 6–12 MΩ when filled with an internal solution of 135 mM KCH_3SO_4, 3.8 mM NaCl, 1 mM $MgCl_2.6H_2O$, 10 mM Hepes, 0.1 mM Na_4EGTA, 0.4 mM Na_3GTP and 2 mM $Mg_{1.5}ATP$ (pH 7.3 with KOH; 290 mosmol l^{-1}). Alexa Fluor 568 or 594 hydrazide sodium salt (20 μM) (Invitrogen, Carlsbad, CA, USA) was added to the internal solution on the day of recording in order to visualize neurons under 2PLSM.

Electrophysiological records were acquired using a computer running Clampex 9 software (Molecular Devices, Palo Alto, CA, USA) connected to a Multiclamp 700B amplifier (Molecular Devices) via a Digidata 1322A digitizer (Molecular Devices). Data were low-pass filtered at 10 kHz and sampled at 50 kHz. Electrode capacitance was compensated on-line. Voltage errors due to series resistance were corrected off-line. A liquid junction potential of 9 mV was subtracted from recordings that employed KCH_3SO_4-based internal solution.

STN neurons were visualized using a fixed stage upright microscope (BX51WI, Olympus, Tokyo, Japan) and a ×60, 0.9 NA water-immersion lens (Olympus). Neurons were imaged at 780–820 nm with 90 MHz pulse repetition and 200 fs pulse duration at the sample plane. The light source was a Chameleon-XR tunable laser (720–950 nm) (Coherent, Glasgow, UK) that was regulated with a Pockels cell electro-optic modulator (model 350–50-02, Con Optics, Danbury, CT, USA). Imaging was carried out using an Ultima 2P dedicated system (Prairie Technologies, Inc., Middleton, WI, USA). Neurons were initially visualized using laser-scanning Dodt contrast imaging (Luigs & Neumann, Ratingen, Germany; Prairie Technologies, Inc.). Upon establishment of the whole-cell configuration, Alexa Fluor dye was allowed to diffuse into the recorded neuron for 10–20 min. High-magnification images of Alexa Fluor-filled dendritic or axonal arbors were then used to guide the placement of further pipettes. Visually guided loose-seal cell-attached dendritic or axonal recordings were made using 6–12 MΩ impedance pipettes prepared as for whole-cell recording except that they were filled with 145 mM NaCl, 10 mM Hepes and 20 μM Alexa Fluor 488 or 568 or 594 hydrazide (pH 7.35 with 1 M NaOH; 300–310 mosmol l^{-1}).

Compartment-selective application of drugs or low $[Na^+]$ external medium was made using similarly prepared pipettes except that they contained 1 μM tetrodotoxin (TTX; Ascent Scientific, Weston-super-Mare, UK) or 1 mM γ-aminobutyric acid (GABA; Tocris Bioscience, Ellisville, MO, USA) dissolved in 145 mM NaCl, 10 mM Hepes and 20 μM Alexa Fluor 488 hydrazide (Molecular Probes; pH 7.35 with NaOH; 300–310 mosmol l^{-1}) or low $[Na^+]$ ACSF, which comprised 136.2 mM *N*-methyl-D-glucamine (NMDG), 13.8 mM NaCl, 2.5 mM KCl, 10 mM Hepes, 10 mM glucose, 2 mM $MgCl_2.6H_2O$, 2 mM $CaCl_2.2H_2O$ and 20 μM Alexa Fluor 488 hydrazide (pH 7.4 with HCl; 300–310 mosmol l^{-1}). Pressure was applied using a Picospritzer II (Parker Hannifin Corp., Cleveland, OH, USA) at 30–60 kPa for 10–50 ms to eject solution. The extent of drug/medium application was estimated by 2PLSM movies of ejected Alexa Fluor 488 and the minimal distance of GABA application from the soma that failed to elicit a response. Using these approaches we estimated that effective drug/medium applications could be restricted to < 20 μm. During GABA application experiments the $GABA_B$ antagonist (2*S*)-3-[[(1*S*)-1-(3,4-dichlorophenyl)ethyl]amino-2 hydroxypropyl](phenylmethyl)phosphinic acid (CGP 55845; Tocris Bioscience) was applied at 2 μM to block $GABA_B$ receptors. Upon completion of electrophysiological experiments, maximum intensity projections of 2PLSM *Z*-series with recording and application pipettes in place were made using 0.5–1 μm focal steps.

Golgi labelling and electron microscopy

Experiments were carried out in four (2 18–20-day-old and 2 adult) Sprague–Dawley rats (Charles River Laboratories). Rats were deeply anaesthetized with sodium pentobarbital (Nembutal, 150 mg kg^{-1}, I.P., Oviation

Pharmaceuticals, Deerfield, IL, USA) before transcardial perfusion with 50–100 ml of phosphate-buffered saline (PBS, 0.01 M, pH 7.4), 250 ml of 2.5% glutaraldehyde and 4% paraformaldehyde in phosphate buffer (PB, 0.01 M, pH 7.4), 250 ml of 4% paraformaldehyde in PB and finally 100 ml of PBS. After perfusion, the STN was sectioned in the sagittal plane at 70 μm (VT1000s, Leica, Bannockburn, IL, USA). Following further washes in PBS, sections were equilibrated in PB and postfixed in 1% osmium tetroxide (Electron Microscopy Sciences, Ft Washington, PA, USA) in 0.1 M PB at pH 7.4 for 30 min. Sections were then further washed before trimming with a razor blade to maximize diffusion of Golgi labelling solutions. The single-section Golgi-impregnation technique was carried out, as previously described (Gabbott & Somogyi, 1984). Briefly, sections were placed in 3.5% $K_2Cr_2O_7$ for 1–3 days followed by 2.5% aqueous $AgNO_3$ for 6–24 h. Sections containing Golgi-impregnated neurons were then gold-toned (Fairen *et al.* 1977). Finally, sections were dehydrated through a graded series of dilutions of alcohol, washed in propylene oxide, infiltrated with resin (Durcupan; Fluka Chemicals, Sigma-Aldrich, St Louis, MO, USA), mounted on glass microscope slides and polymerized at 60°C for 48 h. Golgi-impregnated STN neurons were examined with a Leica DBLM microscope (Leica Microsystems, Wetzlar, Germany) equipped with a ×100 1.25 NA oil-immersion lens and reconstructed using Neurolucida (Microbrightfield, Inc., Williston, VT, USA). Only neurons with extensively filled processes and axons whose entire stained portion remained within single slices were reconstructed. Reconstructions were corrected for an estimated 10% shrinkage due to fixation. In some cases, labelled STN neurons were excised and re-sectioned serially at 50–100 nm (Ultracut E, Leica Microsystems). Ultrathin sections were collected on pioloform-coated slot grids (Electron Microscopy Sciences), stained with lead citrate and then examined and photographed with a transmission electron microscope (Jeol 1200, Jeol USA, Peabody, MA, USA).

Immunocytochemistry

In order to detect ankyrin G in axon initial segments and nodes of Ranvier, STN neurons were filled in slices (derived from 6 rats) in the whole-cell configuration (as described above) with 0.5% biocytin. After filling for 20 min, slices were immersed in 4% paraformaldeyhyde in 0.1 M PB pH 7.4 for 1–2 h. After fixation slices were washed in PBS. Reagents for the detection of ankyrin G and biocytin were diluted in PBS containing 1% bovine serum albumin, 1% normal goat serum and 0.5% Triton X-100 (Sigma-Aldrich). Slices were incubated in 1 : 100 mouse anti-ankyrin G (463; Santa Cruz; Santa Cruz, CA, USA) for 48 h at 4°C and then 1 : 100 Alexa Fluor 488-conjugated goat anti-mouse IgG (Invitrogen) and 1 : 500 Alexa Fluor 594-conjugated streptavidin (Invitrogen) for 2 h at room temperature. Finally, slices were mounted on glass slides in PBS/glycerol and imaged using 2PLSM, as described above.

Data analysis

Electrophysiological data were analysed using Clampfit 10 (Molecular Devices), IgorPro 6 (Wavemetrics, Portland, OR, USA) and Prism 5 (GraphPad Software, San Diego, CA, USA) software. The threshold and maximum rate of rise of somatic action potentials were calculated from averages of 100 action potentials aligned to their peaks. Action potential threshold was detected as the point at which the derivative of the membrane potential (dV/dt) deviated from membrane noise prior to threshold by greater than 2 S.D. Axons and dendrites were measured using the Neuron Morpho plugin for ImageJ (National Institutes of Health, Bethesda, MD, USA). Numerical data are presented as mean ± S.D. An α value of 0.05 was used as the criterion for determining statistically significant differences.

Results

Electrophysiological data collected from 75 neurons were selected for analysis. As previously described, STN neurons exhibited regular autonomous firing, high-frequency firing in response to depolarizing current, a pronounced depolarizing 'sag' in response to hyperpolarizing current, and a rebound depolarization upon termination of hyperpolarizing current (Nakanishi *et al.* 1987*a*; Overton & Greenfield, 1995; Beurrier *et al.* 1999, 2000; Bevan & Wilson, 1999; Song *et al.* 2000; Hallworth *et al.* 2003).

Action potential waveforms recorded in the loose-seal cell-attached configuration are related to the first temporal derivative of the membrane potential

Dual whole-cell somatic and loose-seal cell-attached current-clamp recordings were employed to study the initiation and propagation of action potentials in STN neurons. As previously described (Meeks *et al.* 2005; Teagarden *et al.* 2008), simultaneous dual whole-cell somatic and loose-seal cell-attached somatic recordings ($n = 5$) confirmed that the signal recorded in the loose-seal cell-attached configuration was related to the local capacitive current, and therefore the first temporal derivative of the action potential (Fig. 1). Furthermore, the nature of the loose-seal cell-attached measurement was not altered by the inclusion of 1 μM TTX ($n = 3$; data

not shown) in the recording electrode suggesting that ionic current did not contribute greatly to the signal.

The timing of action potentials in different compartments of neurons has been determined from the relative timing of the peak of the temporal derivative of the somatic membrane potential (dV/dt) and the peak voltage recorded with the loose-seal cell-attached pipette. However, two distinct components may be observed in the temporal derivative of the somatic membrane potential. The first component may correspond to the generation of an action potential in the proximal axon, whereas the second component may represent the delayed generation of an action potential in the somatodendritic compartment (Coombs *et al.* 1957; Fuortes *et al.* 1957; Häusser *et al.* 1995; Colbert & Johnston, 1996; Khaliq & Raman, 2006; Kuba *et al.* 2006; Palmer & Stuart, 2006; Gentet & Williams, 2007; Shu *et al.* 2007; Kole *et al.* 2008). These two components may also be detected in loose-seal cell-attached recordings from the proximal axon with the relative contribution of the somatic component decreasing with distance from the soma. Inferences based on the timing of peaks of the temporal first derivative of the somatic voltage and the loose-seal cell-attached record may therefore be confounded by comparison of different components of action potentials at proximal *versus* distal axonal sites (Meeks & Mennerick, 2007). This problem has been addressed by use of the second temporal derivative of the somatic membrane potential (d^2V/dt^2) in which axonal and somatic components of action potentials are resolved more clearly (Meeks & Mennerick, 2007). In order to compare the timing of similar components of action potentials, we therefore compared the timing of the first peak of the second temporal derivative of the somatic membrane potential with the first/only peak of the first temporal derivative of the loose-seal cell-attached somatic record (dV/dt; $n = 5$; Fig. 1). These recordings confirmed that the first peak of the second temporal derivative of the somatic membrane potential and the first peak of the first temporal derivative of the loose-seal cell-attached somatic record were aligned across the range of loose-seal resistances obtained in this study. This method of comparison was therefore used for subsequent experiments in which whole-cell somatic recordings were combined with 2PLSM-guided loose-seal cell-attached recordings from the axonal and/or dendritic compartments of STN neurons. Axons were distinguished from dendrites as fine calibre aspiny processes, which emerged from the soma or a proximal dendrite, traversed a greater distance than any other process and/or if severed during the slicing procedure formed a characteristic retraction ball at the cut ending. An example of this approach is illustrated in the online Supplemental material (Supplemental Fig. 1). The loose-seal cell-attached configuration was first established on the proximal axon of an STN neuron, 28 μm from

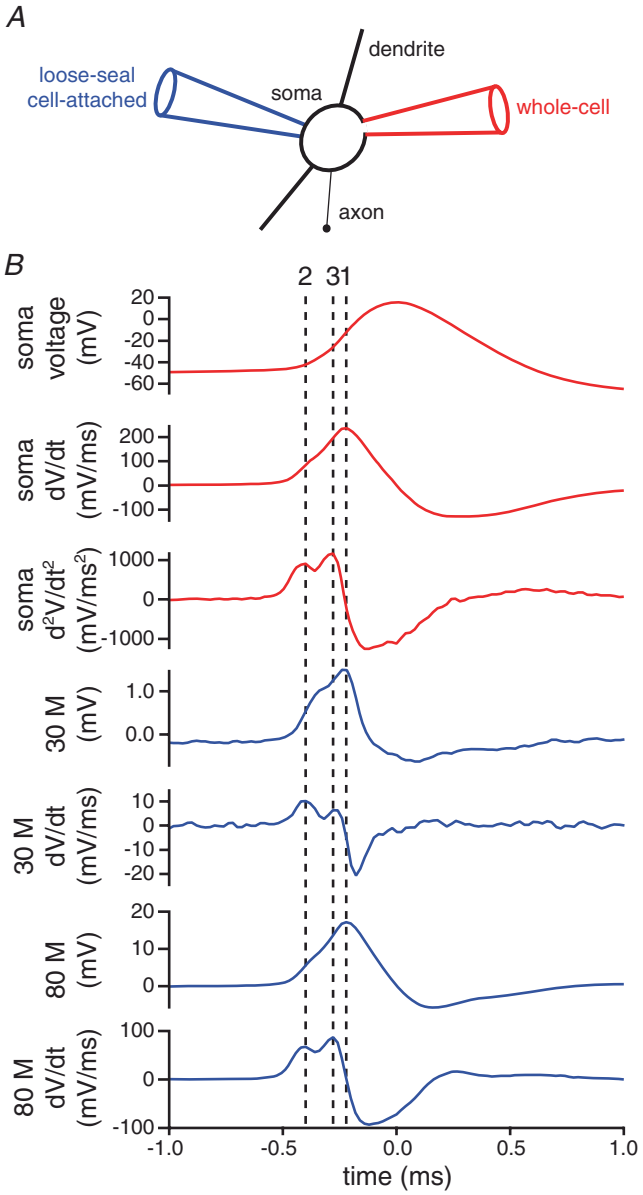

Figure 1. Loose-seal cell-attached recordings are related to the first temporal derivative of the action potential
A, schematic illustration of the recording configuration. Autonomously generated action potentials were recorded simultaneously from the soma of a STN neuron using a pipette in the whole-cell configuration (red pipette) and a pipette in the loose-seal cell-attached configuration (blue pipette). *B*, action potential-triggered averages of 100 action potentials recorded in the whole-cell (red traces) and loose-seal cell-attached (blue traces) configurations. Loose-seal cell-attached records were obtained for seal resistances of 30 and 80 MΩ, which approximate the range of resistances obtained with this technique. Note the alignment (line 1) of the peak of the first temporal derivative (dV/dt) of the whole-cell record and the loose-seal cell attached records. Note also the alignment of the first (line 2) and second (line 3) peaks of the second temporal derivative (d^2V/dt^2) of the somatic whole-cell record with the first and second peaks of the first temporal derivative (dV/dt) of the loose-seal cell-attached records, respectively. Similar results were obtained in each recorded neuron ($n = 5$).

the soma (Supplemental Fig. 1*A*). The loose-seal recording pipette was then repositioned on a dendrite 43 μm from the soma (Supplemental Fig. 1*B*). The axonal action potential preceded the somatic action potential by 0.04 ms, whereas the dendritic action potential followed the somatic action potential by 0.18 ms.

Autonomously generated action potentials are initiated in the proximal axon of STN neurons

In the majority of neurons, axons originate from the soma or a proximal dendrite. In some neurons, e.g. midbrain dopamine neurons, axons may emerge from a dendrite up to several hundred micrometres from the cell body. In these cases, the relative timing of action potentials in dendrites can differ depending on whether action potentials in axon- or non-axon-bearing dendrites are recorded (Häusser *et al.* 1995; Gentet & Williams, 2007). This issue was first addressed through analysis of maximum intensity projections of 2PLSM *Z*-series of 38 STN neurons that had been filled with Alexa Fluor dye via a somatic whole-cell electrode. In 29 of 38 neurons axons originated from the soma. In 9 cases axons emerged from a proximal dendrite 8.6 $\pm$ 5.2 μm from the soma. These data are concordant with previous observations (Kita *et al.* 1983*b*; Afsharpour, 1985) and demonstrate that the axons of STN neurons originate from or very close to the soma.

Axonal and/or dendritic compartments were then sampled at varying distances from the soma using the technique outlined above to determine the relative timing of action potentials in STN neurons. Action potentials recorded from the dendrites of STN neurons followed somatic action potentials over the range of distances tested (Fig. 2*A* and *C*; 43–226 μm; average = 87 $\pm$ 43 μm; n = 14). Axons (n = 24) were recorded at sites ranging from 14 to 836 μm (average = 208 $\pm$ 219 μm) from the

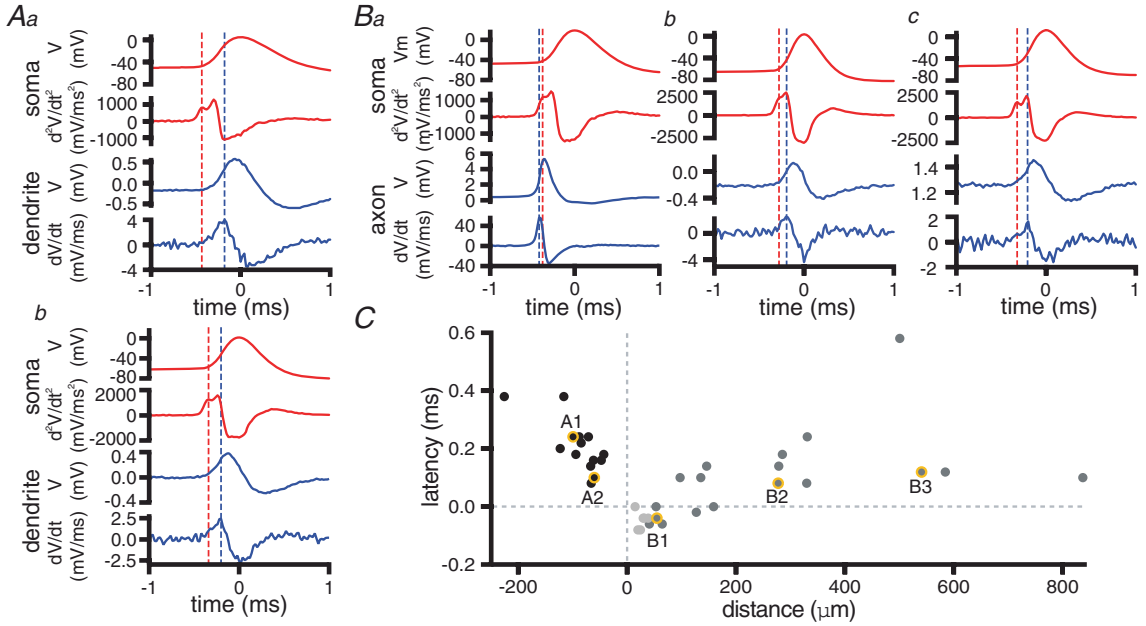

Figure 2. Action potentials are first detected in the proximal axon
A, action potential-triggered averages of 100 action potentials recorded with somatic whole-cell (red traces) and dendritic loose-seal cell-attached (blue traces) electrodes. Dendritic electrodes were positioned 100 μm (*a*) and 61 μm (*b*) from the soma. Note that the peak of the first temporal derivative of the dendritic loose-seal recording (blue dotted line) follows the first peak of the second temporal derivative of the whole-cell record (red dotted line) and the delay is greater for the more distal dendritic recording. *B*, action potential-triggered averages of 100 action potentials recorded with somatic whole-cell (red traces) and axonal loose-seal cell-attached (blue traces) electrodes. Axonal electrodes were positioned 54 μm (*a*), 277 μm (*b*) and 540 μm (*c*) distal to the soma. Note that the peak of the first temporal derivative of the most proximal axonal loose-seal recording (blue dotted line) precedes the first peak of the second temporal derivative of the whole-cell record (red dotted line). At more distal axonal recording sites action potentials were relatively delayed compared to somatic action potentials. *C*, latency of the first peak of the second derivative of the somatic action potential relative to the peak of the first derivative of the cell-attached record plotted against the distance of the loose-seal cell-attached recording electrode from the soma. Distances of cell-attached recordings from the soma are plotted as negative and positive for dendrites and axons, respectively. The points drawn from the examples shown in *A* and *B* are highlighted. Axonal recordings from sites of truncation or from intact parts of axons are denoted by light and dark grey points, respectively.

soma. In contrast to dendritic recordings, action potentials recorded from STN axons within 100 μm of the soma preceded, or were synchronous with, somatic action potentials (Fig. 2*B* and *C*).

In order to determine the morphological properties of the proximal axon where action potentials were first detected, the Golgi labelling technique was applied. Observations were made in juvenile rats (P18–20), in which the majority of electrophysiological recordings were made, and in adult (P53) rats to determine whether the length of the axon initial segment changes during development. Analysis was restricted to neurons in which the labelled axon remained entirely within the section. The distance from the soma to the cessation of axonal Golgi labelling was not significantly different in juvenile and adult rats (Fig. 3; juvenile $= 38 \pm 12$ μm, $n = 12$; adult $= 35 \pm 5$ μm, $n = 11$, $P = 0.559$, Mann–Whitney U test). Correlated light and electron microscopy confirmed in each of two neurons examined that Golgi labelling ceased at the onset of myelination (Fig. 3).

In order to determine the location of the first node of Ranvier, ankyrin G labelling was detected in six STN neurons labelled for biocytin. Ankyrin G labelling was noted in the axon initial segment and nodes of Ranvier

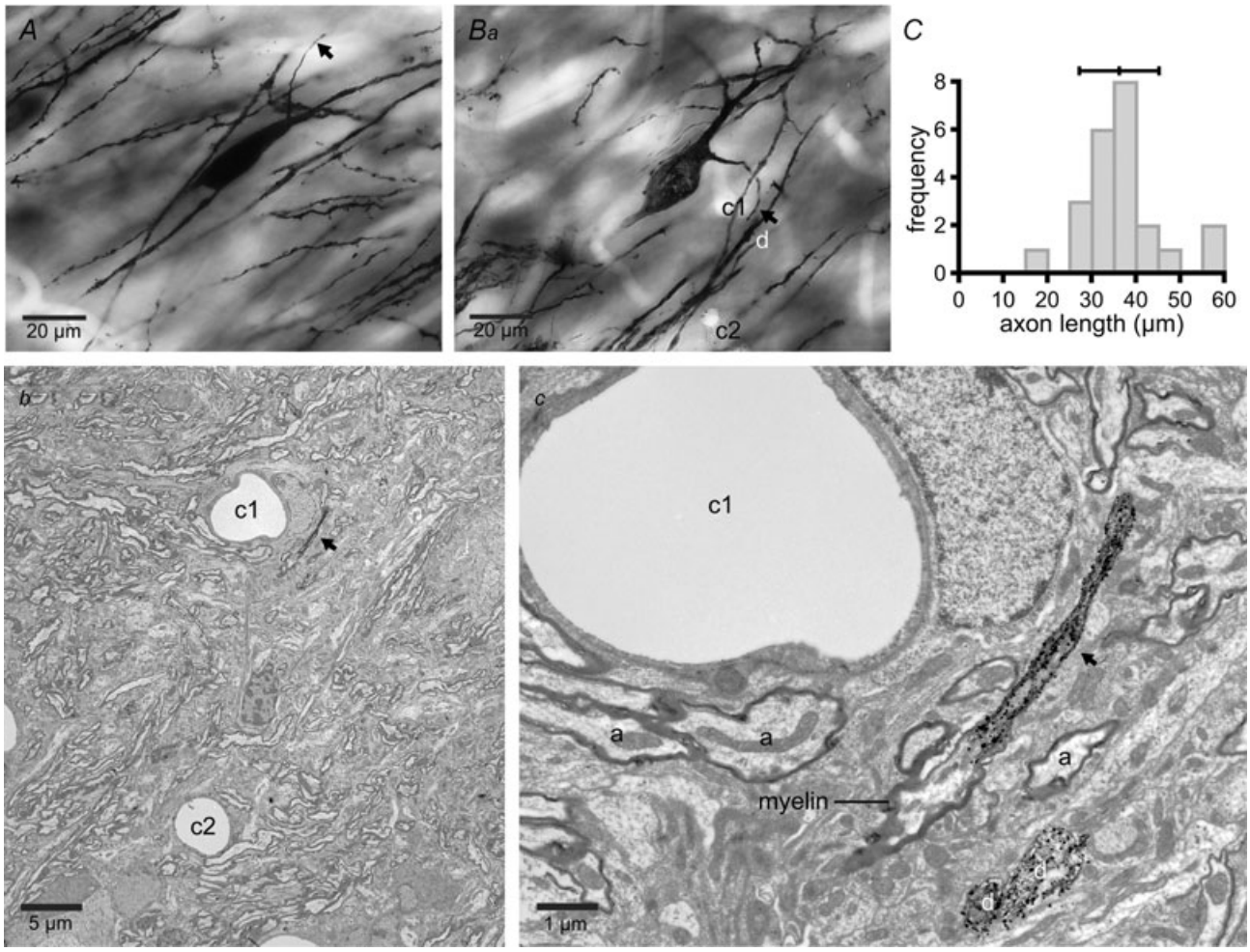

Figure 3. Golgi labelling of the axon initial segment
A and *B*, photomicrographs of STN neurons showing Golgi impregnation of the unmyelinated initial segment of the axon only. Golgi impregnation ceased 30.7 μm from the soma in *A* and 38.2 μm from the soma in *B*. The axons are marked with arrows. *Bb* and *c*, electron microscopic analysis of the neuron in *Ba* (and *A*, not illustrated) confirmed that Golgi labelling ceased at the beginning of the myelin sheath. *Bb*, low magnification electron micrograph illustrating capillaries (c1 and c2), which act as points of registration between the light (*Ba*) and electron micrographs (*Bb* and *c*). *Bc*, higher magnification micrograph illustrating the end of the Golgi-labelled axon initial segment and the beginning of the unlabelled myelinated section of axon. Golgi-labelled dendrites (d) act as further points of registration between *Ba* and *c*. Other unlabelled myelinated axons (a) are denoted in *Bc*. *C*, frequency–axon initial segment length histogram for 23 (11 adult, 12 juvenile) neurons. Mean $\pm$ S.D. is indicated above the graph.

of biocytin-filled STN neurons (Fig. 4). The zone of initial segment labelling was $39 \pm 6\,\mu$m in length. The first and second nodes of Ranvier were detected at $105 \pm 19\,\mu$m and $181 \pm 31\,\mu$m from the soma, respectively. Nodes were also noted at the branch points of axons (Fig. 4*B*). Taking the electrophysiological, Golgi labelling and immunocytochemical data together, our findings indicate that action potentials were first detected in a region that most closely corresponded to the axon initial segment.

The velocity of action potential conduction following initiation was then compared using linear regression of latency against distance for axons and dendrites. Fits were restricted to axonal recordings $> 100\,\mu$m from the soma. Visual inspection and linear regression suggested that axonal conduction velocity was greater than dendritic conduction velocity (axonal $= 4.9\,\mathrm{m\,s^{-1}}$, $r = 0.29$, $P = 0.330$; dendritic $= 0.69\,\mathrm{m\,s^{-1}}$, $r = 0.75$, $P = 0.002$). The relatively poor fit to the axonal latencies may result from neuronal heterogeneity and/or the variable propagation velocity of action potentials at a variety of distances from nodes (Granata & Kitai, 1989; Kita & Kitai, 1991; Palmer & Stuart, 2006).

Autonomously generated action potentials are faithfully propagated in STN neurons

In order to determine whether action potentials are reliably propagated in STN neurons, action potentials detected in the proximal axon (mean distance $= 38 \pm 19\,\mu$m, distance range $= 14$–$64\,\mu$m; $n = 8$) by loose-seal cell-attached recording were first used to determine whether a corresponding action potential was detected in the somatic whole-cell record. Action potentials were discriminated in the loose-seal cell-attached recording when the peak-to-trough amplitude in any given 1.5 ms window exceeded the mean by 2 S.D. Each action potential detected in this manner was also confirmed by visual inspection. The amplitudes of axonal action potentials exhibited a narrow normal distribution in each neuron. These action potentials were then used to detect a corresponding action potential in the somatic compartment. In each neuron ($n = 8$) there was a 100% probability of detecting an action potential with the somatic recording electrode (axon: frequency $= 7.6 \pm 3.4$ Hz, CV $= 0.10 \pm 0.08$; soma: frequency $= 7.6 \pm 3.4$ Hz, CV $= 0.10 \pm 0.08$). Furthermore, the amplitudes of somatic action potentials were consistently large and also exhibited a narrow normal distribution in each neuron. Severely truncated action potentials, which would indicate failures of proximal axonal action potentials to lead to the generation of somatic action potentials were not observed (Fig. 5*A*). These data suggest that action potentials, which are initiated in the proximal axon, invariably lead to the generation of full amplitude somatic action potentials.

Action potentials recorded with somatic whole-cell electrodes were then used to search for corresponding action potentials in loose-seal cell-attached distal axonal records, as described above. In each neuron ($n = 7$) there was a 100% probability of detecting a corresponding action potential in the distal axon (mean distance $= 296 \pm 181\,\mu$m; distance range $= 135$–$584\,\mu$m; soma: frequency $= 7.0 \pm 3.3$ Hz, CV $= 0.36 \pm 0.34$; axon frequency $= 7.0 \pm 3.3$ Hz, CV $= 0.36 \pm 0.34$). The amplitudes of somatic and axonal action potentials in each recorded neuron also exhibited narrow normal distributions (Fig. 5*B*).

Finally, action potentials recorded with somatic whole-cell electrodes were used to search for corresponding action potentials in loose-seal cell-attached dendritic records. In each neuron ($n = 11$) there was also a 100% probability of detecting a corresponding action potential in the dendrite (mean distance $= 79 \pm 27\,\mu$m, distance range $= 43$–$123\,\mu$m; soma: frequency $= 8.6 \pm 4.0$ Hz, CV $= 0.13 \pm 0.17$; dendrite: frequency $= 8.6 \pm 4.0$ Hz, CV $= 0.13 \pm 0.17$) and the amplitudes of somatic and dendritic action potentials in each recorded neuron also exhibited narrow normal distributions (Fig. 5*C*).

Propagation of action potentials at axonal or dendritic branches can fail intermittently due to the extra capacitive load of branch points (Grossman *et al.* 1979; Debanne *et al.* 1997; Debanne, 2004). However, in several cases axons (Fig. 5*B*; $n = 2$ of 7) and dendrites (Fig. 5*C*; $n = 11$ of 11) were recorded beyond branch points and in these cases propagation was also 100% reliable. Taken together, these data suggest that autonomously generated action potentials propagate with high reliability into the axonal and dendritic compartments of STN neurons.

Action potential properties are unaffected by axon truncation

As described above, the axons of recorded STN neurons were often truncated at the slice surface. We used the variability in the length of axons to further investigate the autonomous generation of action potentials. Because our previous experiments indicated that the initiation of action potentials occurs within the proximal axon, we hypothesized that axonal truncation at more distal sites would not affect action potential generation, whereas truncation within the region of initiation would. Autonomously active STN neurons were recorded, filled with Alexa Fluor dye and imaged using 2PLSM, as described above. Axonal lengths ranged from 14 to $822\,\mu$m, $n = 39$. For axons greater than $100\,\mu$m in length it was often not possible to follow them to their point of truncation/termination. Figure 6*A* illustrates examples

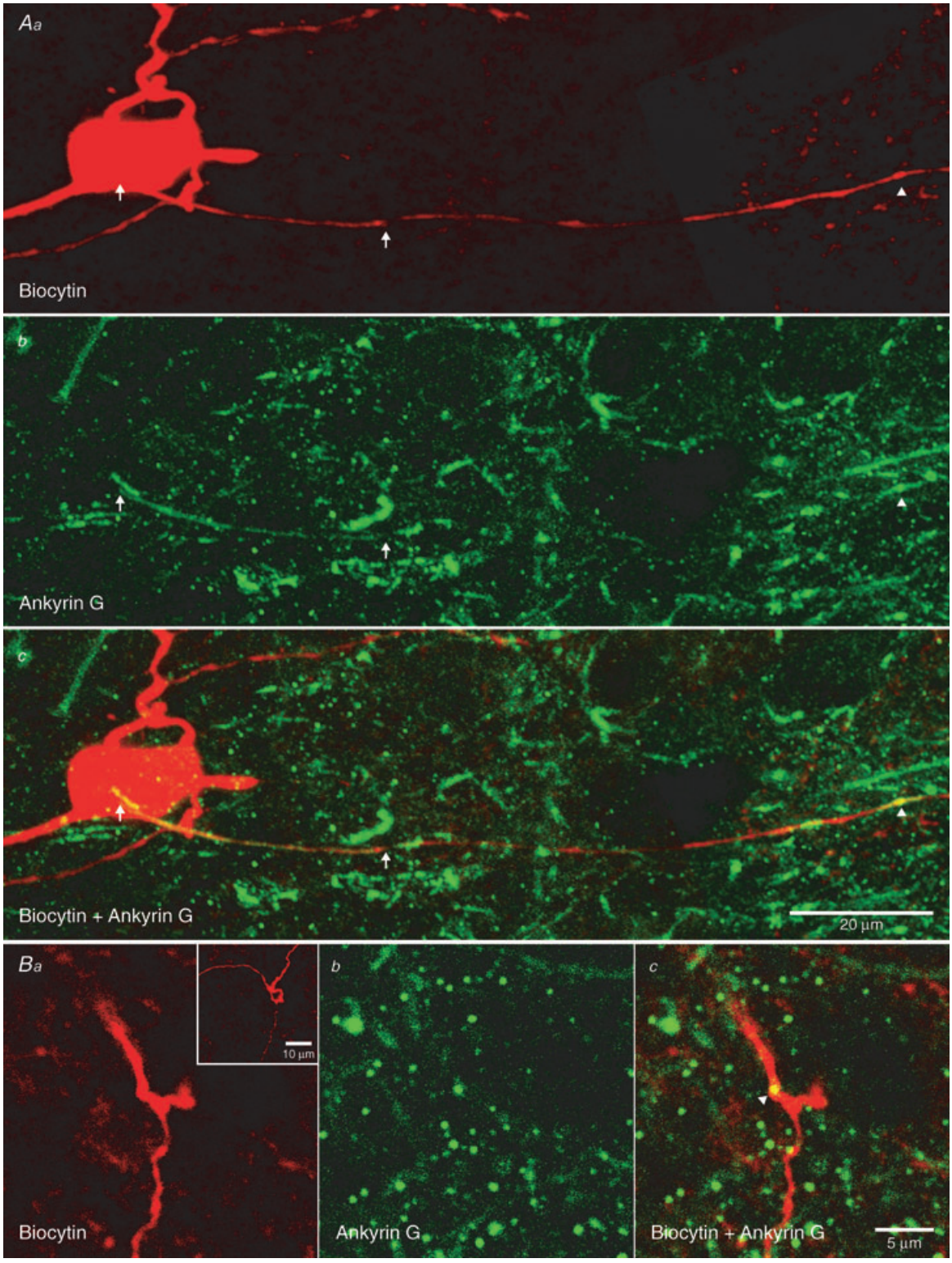

Figure 4. Axonal expression pattern of ankyrin G
2PLSM images of biocytin- (red) and ankyrin G-labelled (green) STN neurons. *Aa–c*, ankyrin G labelling was detected along the axon initial segment (left arrows denote start and right arrows denote the end of labelling) and at the presumptive first node of Ranvier (arrowhead) of the biocytin-labelled neuron. The scale in *Ac* also applies to *Aa* and *Ab*. *Ba–c*, ankyrin G labelling at a proximal axonal branch point of another biocytin-labelled STN neuron (arrowhead). Scale bar in *Bc* also applies to *a* and *b*. *Ba* inset, full *Z*-stack through the axonal branch point.

of neurons with a range of axonal lengths. However, gross differences in the shape of autonomously generated action potentials or their first or second temporal derivatives were not observed in these neurons or across the sample population as a whole (Fig. 6*B*). There was also no significant correlation between axonal length and action potential threshold ($r = -0.130$, $P = 0.429$, Fig. 6*C*) or maximum rate of rise ($r = 0.178$, $P = 0.277$, Fig. 6*D*) of autonomously generated action potentials across 39 neurons tested. Comparison of neurons with axons truncated greater than 100 μm from the soma with axons truncated less than 100, 50 or 25 μm from the soma also revealed no significant difference in the threshold or maximum rate of action potentials (threshold: $> 100\,\mu\text{m} = -53.0 \pm 2.4$ mV, $n = 17$; $< 100\,\mu\text{m} = -51.7 \pm 3.1$ mV, $n = 22$; $< 50\,\mu\text{m} = -52.4 \pm 3.4$ mV, $n = 15$; $< 25\,\mu\text{m} = -52.1 \pm 5.1$ mV, $n = 5$; ANOVA, $P = 0.661$; Dunnett's *post hoc* multiple comparison test, $P > 0.05$ for each pairwise comparison with axons $> 100\,\mu$m) (maximum rate of rise of action potentials: $> 100\,\mu\text{m} = 316.6 \pm 95.3$ mV ms^{-1}, $n = 17$; $< 100\,\mu\text{m} = 321.3 \pm 82.6$ mV ms^{-1}, $n = 22$; $< 50\,\mu\text{m} = 325.8 \pm 95.1$ mV ms^{-1}, $n = 15$; $< 25\,\mu\text{m} = 310.7 \pm 76.9$ mV ms^{-1}, $n = 5$; ANOVA, $P = 0.985$; Dunnett's

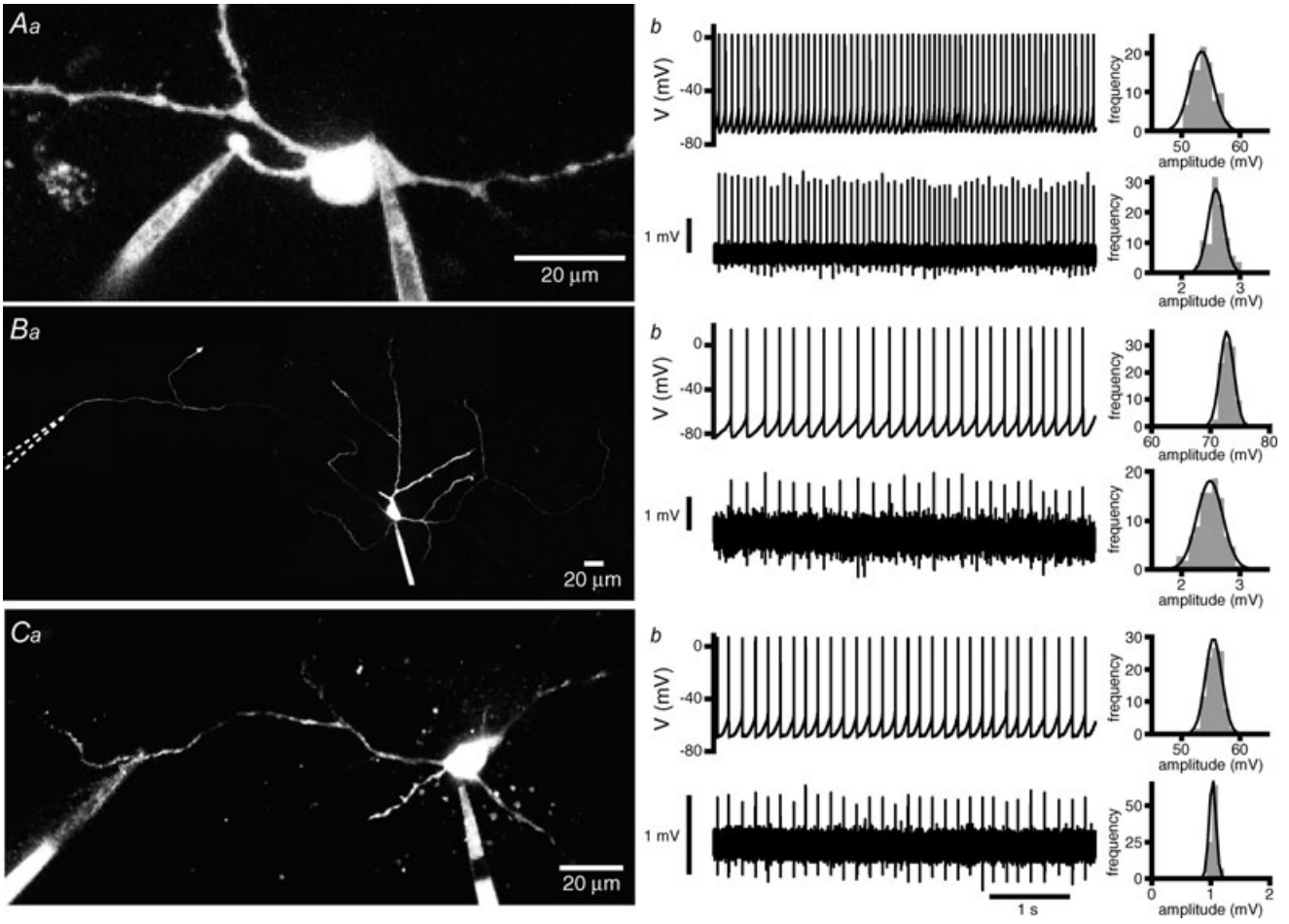

Figure 5. Autonomously generated action potentials are faithfully propagated throughout axonal and somatodendritic compartments
Aa, Ba and *Ca*, maximum intensity projections of 2PLSM *Z*-series of STN neurons recorded simultaneously in the whole-cell somatic and loose-seal cell-attached axonal (*Aa* and *Ba*) or dendritic (*Ca*) configurations. Loose-seal cell-attached electrodes were placed 29 μm (*Aa*), 584 μm (*Ba*), and 117 μm (*Ca*) from the soma. *Ab, Bb* and *Cb*, corresponding whole-cell (upper panels) and loose-seal cell-attached records (lower panels). Autonomously initiated action potentials propagated with 100% reliability into somatic, distal axonal and distal dendritic compartments. Note that distal axonal and dendritic loose-seal cell-attached recordings were made beyond axonal and dendritic branch points. The amplitude of each somatic action potential was large and consistent in each neuron. The amplitudes of loose-seal cell-attached recorded axonal and dendritic action potentials were similarly consistent. Frequency/amplitude histograms together with fits (black line) to normal distributions are illustrated to the right of each recording.

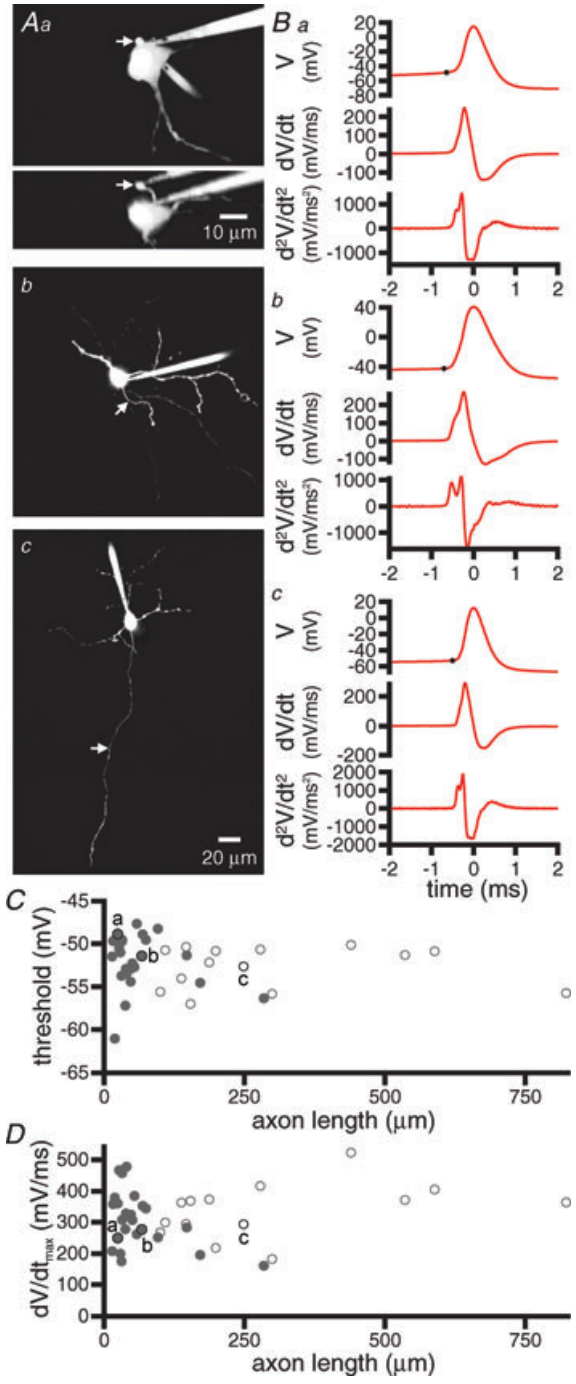

Figure 6. Axonal truncation does not affect the shape, threshold or maximal rate of rise of autonomously generated action potentials

A, maximum intensity projections of 2PLSM *Z*-series through STN neurons with axons truncated at 24 μm (*Aa*) and 67 μm (*Ab*) or intact for at least 248 μm (*Ac*). An orthogonal projection is also illustrated for *Aa*. The scale bar in panel *Ac* also applies to *Ab*; axons are highlighted with arrows. *B*, spike-triggered averages of 100 action potentials taken from somatic whole-cell recordings from the cells shown in *A*. Dots mark threshold. The first and second derivatives of each trace are also shown. *C*, action potential thresholds for 39 neurons with axons truncated at varying lengths. *D*, maximum rate of rise (dV/dt_{max}) of action potentials from the same neurons, as shown in *C*. For both *C* and *D*, open symbols represent axons, which could not be followed for their entire length, the distance shown in these cases represents the maximum length of the axon that could be detected with 2PLSM. The lettered highlighted points (a-c) correspond to the cells shown in *A* and *B*. Note that the shape, threshold and maximum rate of rise of action potentials are similar for STN neurons with variable degrees of transection.

post hoc multiple comparison test, $P > 0.05$ for each pairwise comparison with axons $> 100\,\mu$m). Taken together, these data suggest that the axon initial segment and somatic compartment of STN neurons express a large reserve of Na_v channels for the autonomous generation of action potentials.

Autonomous action potential generation is most sensitive to reduction of proximal axonal Na_v channel current

Previous studies have indicated that action potentials are initiated in a region that either possesses a higher density of Na_v channels (Kole *et al.* 2008), and/or possesses Na_v channels with specialized gating properties (Colbert & Pan, 2002; Astman *et al.* 2006; Castelli *et al.* 2007). Our hypothesis was therefore that the autonomous generation of action potentials in STN neurons would be most sensitive to the manipulation of Na_v channel current in the axonal region of initiation. In order to test this hypothesis, extracellular $[Na^+]$ was lowered in the vicinity of specific regions of STN neurons through the local application of Hepes-buffered ACSF in which Na^+ was partially replaced with NMDG (control extracellular $[Na^+] = 126$ mM; reduced extracellular $[Na^+] = 13.8$ mM). Figure 7*A* illustrates the responses of an autonomously active STN neuron to low $[Na^+]$ ACSF applied by 50 ms pressure-pulses at five different locations (Fig. 7*B*). Application of low $[Na^+]$ ACSF was considered to have had a significant effect on initiation if the threshold of action potentials that occurred immediately following application were significantly different to the threshold of action potentials generated during control trials (10 trials of each, interspersed as 5 control; 5 low $[Na^+]$ ACSF; 5 control; 5 low $[Na^+]$ ACSF; Mann–Whitney *U* test). In this example, application of low $[Na^+]$ ACSF to the soma, proximal dendrite, or axon 40 μm distal to the soma had no significant effect on the autonomous generation of action potentials. However, applications to the axon 15 μm or 30 μm distal to the soma significantly depolarized the threshold of action potentials generated immediately following application. Action potentials that followed low $[Na^+]$ ACSF application were also relatively delayed compared to action potentials recorded in control trials. Application of low $[Na^+]$ ACSF to the proximal axon led to a significant depolarization of action potential threshold in each neuron tested (axon

0–20 μm from the soma: control = –51.5 ± 3.8 mV, low [Na^+] ACSF = –47.9 ± 5.1 mV, $n = 7$, $P = 0.016$, Wilcoxon signed ranks test; axon 20–40 μm from the soma: control = –52.4 ± 3.7 mV, low [Na^+] ACSF = –49.8 ± 5.1 mV, $n = 8$, $P = 0.008$,Wilcoxon signed ranks test).

Application of low [Na^+] ACSF to the soma had more variable effects on the threshold of action potentials. No significant effect was observed in 3 of the 6 neurons tested at this site but in the 3 other neurons the greatest effect of all sites tested was at the soma. This disparity could reflect difficulty in restricting the low

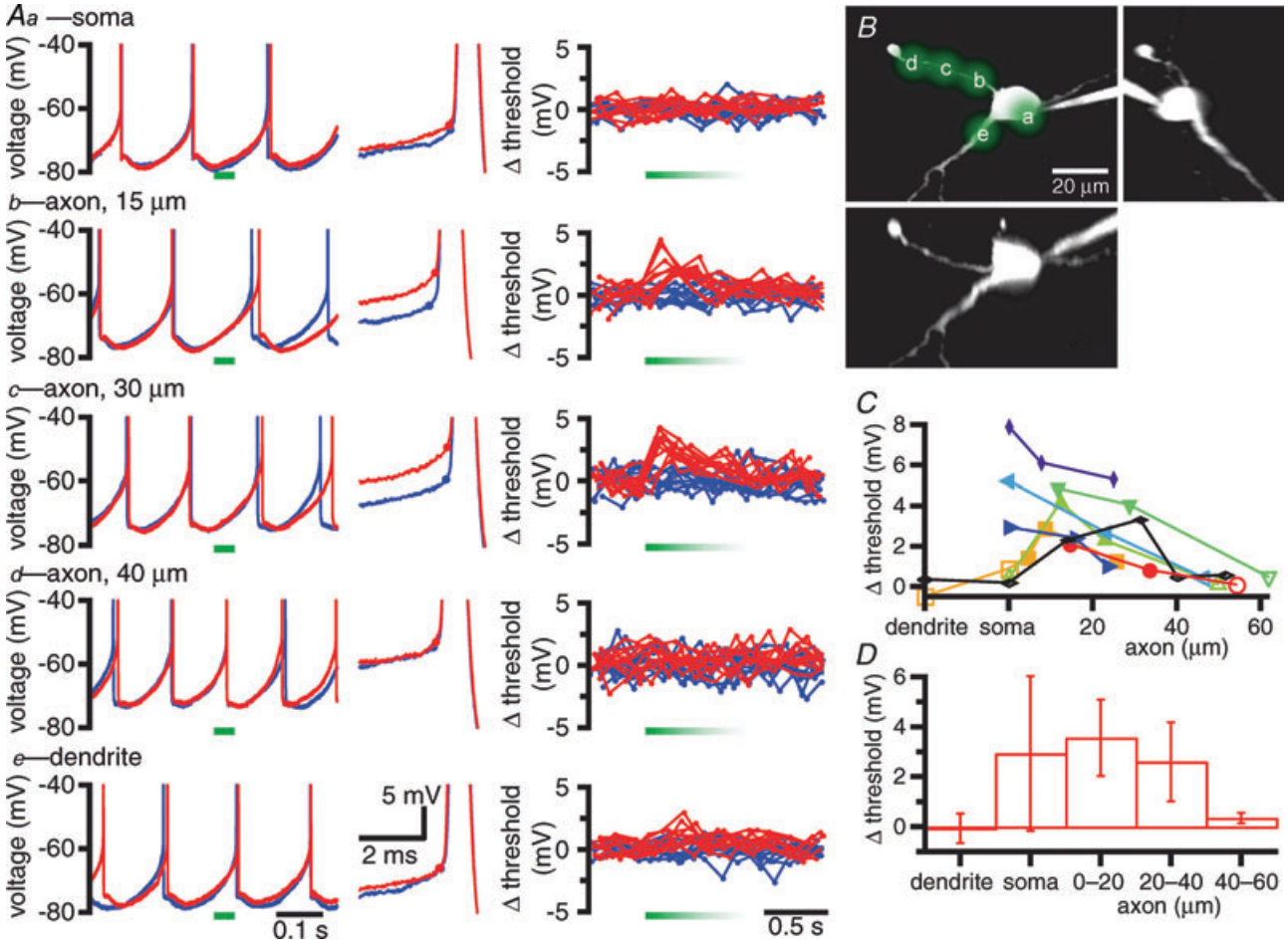

Figure 7. Reduction of extracellular [Na^+] in the vicinity of the axon initial segment or cell body depolarizes the threshold of autonomously generated action potentials
A, effects of local application of low [Na^+] ACSF at the soma (*Aa*), a dendrite (*Ae*), and at three axonal locations (*Ab–d*) on the autonomous generation of action potentials. Left-hand panels, overlaid traces from control trials (blue) and trials in which low [Na^+] ACSF was pressure-pulse-applied for 50 ms (red traces; time of application marked with horizontal green bars). Middle panels, zoom of single action potentials from control (blue) and low [Na^+] ACSF (red) trials aligned to the peak of each action potential. Action potential thresholds are marked with a dot on each trace. Right-hand panels, plots of the deviation of action potential threshold from mean threshold (measured in control traces) for all action potentials in 10 control trials (blue) and 10 trials of low [Na^+] ACSF application (red). Applications of low [Na^+] ACSF began at the start of the green bars. The length of the green bars approximates the duration of locally reduced extracellular [Na^+] as assessed by the fluorescence of ejected Alexa Fluor 488. *B*, the sites of low [Na^+] ACSF used in *A* superimposed on a maximum intensity projection of a 2PLSM *Z*-series of the neuron. Orthogonal (*X* and *Y*) projections are also illustrated. *C*, summary of the effect of low [Na^+] ACSF application on action potential threshold in 8 cells. The data shown in black are from the example illustrated in *A* and *B*. Filled symbols represent sites of application that increased the threshold of action potentials compared to control trials, as measured by the Mann–Whitney *U* test. Open symbols represent sites of application that had no significant effect on threshold. *D*, mean ± S.D. effect of low [Na^+] ACSF application on action potential threshold for dendritic, somatic and axonal sites.

$[Na^+]$ ACSF to the soma when the axon emerges from the soma at specific orientations relative to the application pipette or an underlying heterogeneity in the location of Na_v channels in STN neurons. Across all 6 neurons tested there was, however, a significant depolarization of action potential threshold following the application of low $[Na^+]$ ACSF to the soma (control $= -50.0 \pm 4.7$ mV, low $[Na^+]$ ACSF $= -47.1 \pm 6.6$ mV, $n = 6$, $P = 0.031$, Wilcoxon signed ranks test).

Low $[Na^+]$ ACSF application to the dendrites or distal axon (greater than 40 μm from the soma) of STN neurons had no significant effect on action potential threshold in each neuron tested (dendrites: control $= -57.1 \pm 0.6$ mV, low $[Na^+]$ ACSF $= -57.2 \pm 0.0$ mV, $n = 2$; axon > 40 μm from soma: control $= -53.7 \pm 3.8$ mV, low $[Na^+]$ ACSF $= -53.4 \pm 3.8$ mV, $n = 5$).

Hypothetically, reduction of extracellular $[Na^+]$ could have effects on ionic fluxes other than those mediated by Na_v channels. Thus, to ensure that the results obtained through low $[Na^+]$ ACSF application were attributable to a reduction in Na^+ current through Na_v channels, further experiments were performed using the compartment-selective application of the Na_v channel blocker TTX (1 μM; Fig. 8). The effect of local 50 ms applications of TTX on action potential threshold had a slower time course than local Na^+ reduction. Therefore changes in threshold were averaged from action potentials that occurred in the second following application. TTX application at any given location was considered effective if the threshold of action potentials in the first five trials of TTX application exhibited a statistically significant change compared to five control trials prior to the application of TTX (Mann–Whitney *U* test). The effect of TTX application was also slower to reverse than low $[Na^+]$ ACSF. The effects of TTX often accumulated over successive trials 30 s apart, and took minutes to reverse (full reversal was rarely achieved). An example of a neuron in which 1 μM TTX was applied locally to four sites is illustrated in Fig. 8. Application at a site 24 μm from the soma was the most effective at elevating action potential threshold, leading to a complete cessation of firing by the 9th trial (Fig. 9*Ab*). TTX application at the soma or axon 44 μm from the soma also elevated action potential threshold, but to a lesser extent. Application at a dendrite did not significantly affect the threshold for action potential generation (Fig. 8).

Across the sample population, application of TTX to the proximal 20 μm of the axon had a significant effect on action potential threshold in each cell tested (change in threshold $= 2.0 \pm 1.2$ mV, $n = 5$). Application of TTX to the axon 20–40 μm from the soma produced a significant change in threshold in 2/4 cells tested (change in threshold $= 2.0 \pm 2.1$ mV, $n = 4$). Application of TTX to

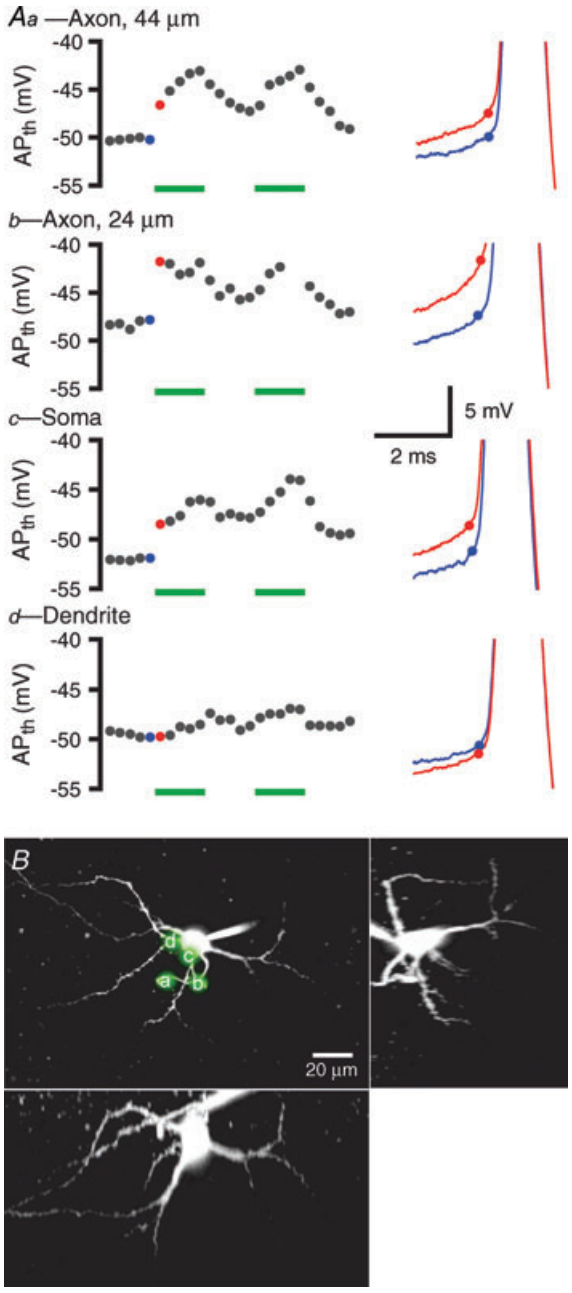

Figure 8. Proximal axonal and somatic application of TTX depolarizes the threshold of autonomously generated action potentials
A, responses of a representative neuron to 50 ms pressure applications of 1 μM TTX at two axonal sites (*a*, 44 μm from the soma; *b*, 24 μm from the soma), the soma (*c*), and a dendrite (*d*). The left-hand panels show the average action potential threshold (AP_{th}) from individual 1 s trials during which TTX was or was not applied. Trials were repeated every 30 s with 5 TTX trials interleaved with 5 control trials. Trials in which TTX was applied are marked with green bars. The blue and red dots correspond to examples in the right-hand panels. The right-hand panels show overlaid action potentials from control (blue) and TTX (red) trials. Dots denote threshold. *B*, the sites of TTX application in *A* (a-d) are superimposed on a maximum intensity projection of a 2PLSM *Z*-series of the neuron. Orthogonal (*X* and *Y*) projections are also illustrated.

the axon 40–60 μm from the soma significantly elevated action potential threshold in 3/6 cells tested (change in threshold = 2.0 ± 2.2 mV, $n = 6$). Axonal sites greater than 60 μm from the soma were tested in 3 cells. The most distal site of axonal application of TTX that significantly elevated action potential threshold was 70 μm from the soma (change in threshold = 1.7 mV). Applications at axonal sites 76 μm and 107 μm from the soma did not affect threshold. Applications of TTX to the soma had a significant effect in 5/8 cells tested (change in threshold = 2.4 ± 2.4 mV, $n = 8$). There was no effect on action potential threshold when TTX was applied to the dendrites of two neurons. Taken together these data demonstrate that manipulation of Na_v channels in the axon initial segment most consistently elevates action potential threshold. These data are also consistent with the conclusion that Na_v channels in the axon initial segment and soma are primarily responsible for the autonomous initiation of action potentials in STN neurons.

Somatodendritic applications of GABA generate larger and faster currents than axonal applications of GABA

$GABA_A$ receptor-mediated IPSPs can both deactivate and deinactivate Na_v channels that underlie the autonomous activity of STN neurons (Bevan *et al.* 2002; Baufreton *et al.* 2005). In many cell types action potential generation

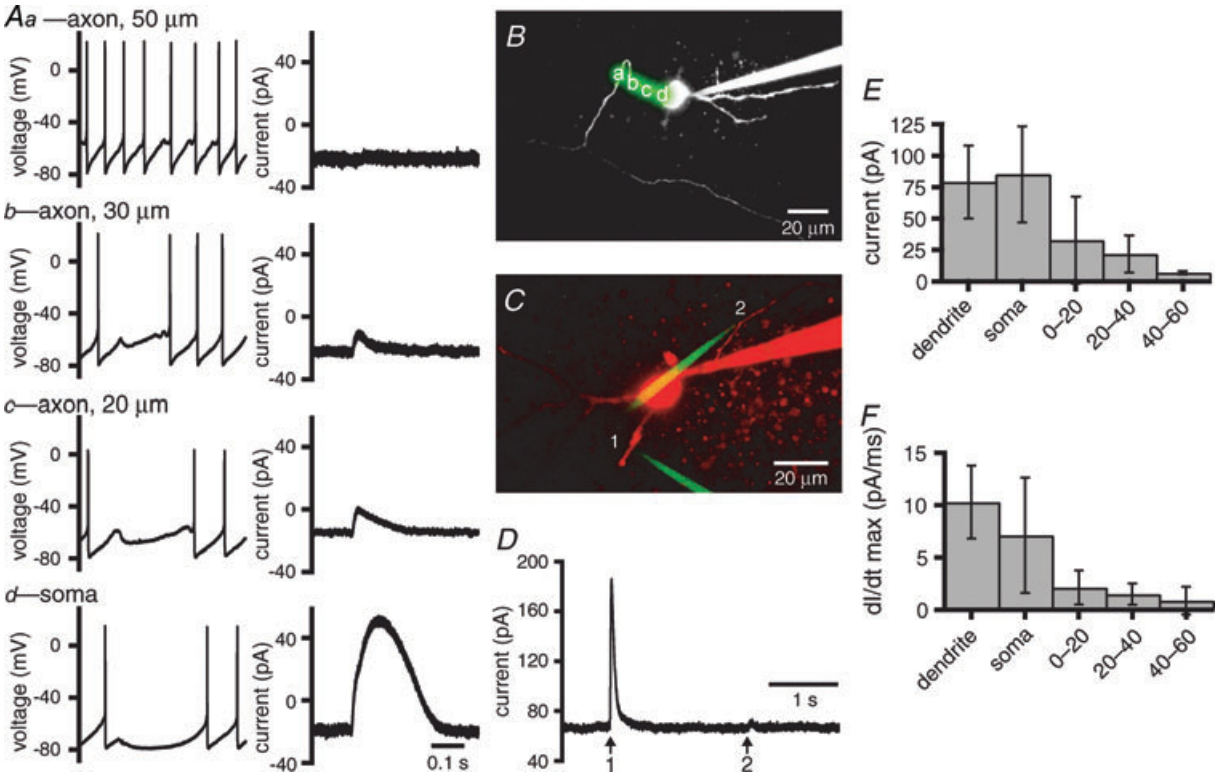

Figure 9. Somatodendritic application of GABA evoked larger and faster $GABA_A$ receptor-mediated currents than axonal application of GABA

A, example recordings illustrating the effects of 10 ms pressure applications of 1 mM GABA to three axonal sites (*a*–*c*) and the soma (*d*). In current-clamp mode (left-hand panels), the greatest hyperpolarization was generated by application of GABA to the soma. The magnitude of hyperpolarization decreased with progressively more distal axonal applications of GABA. In voltage-clamp mode (holding voltage –70 mV; right-hand panels) outward current following application of GABA was greatest for somatic application and decreased in magnitude with progressively more distal axonal applications. *B*, maximum intensity projection of a 2PLSM *Z*-series of the neuron in *A* with locations of GABA application (a–d) highlighted. *C–D,* GABA application at the dendrite (1) and axon (2) of another STN neuron. *C*, maximum intensity projection of a 2PLSM *Z*-series of the neuron with locations of GABA application (1–2) highlighted. The neuron (red) was filled with Alexa Fluor 568 hydrazide. The GABA ejection pipettes (green) contained Alexa Fluor 488 hydrazide. *E*, population data, peak amplitude of outward current that was elicited following 10 ms applications of 1 mM GABA to dendritic, somatic and axonal (0–60 μm from soma) sites. *F*, population data, maximal rate of increase of GABA-evoked current (d*I*/d*t* max) for dendritic, somatic and axonal (0–60 μm from soma) sites of application.

is tightly regulated by $GABA_A$ receptor-mediated synaptic inputs that are directed to somatodendritic and/or axonal compartments (Buhl *et al.* 1995; Miles *et al.* 1996; Häusser & Clark, 1997; Pouzat & Hestrin, 1997; Person & Perkel, 2005; Szabadics *et al.* 2006). The available evidence suggests that STN neurons receive GABAergic synaptic inputs that are directed to their somatodendritic but not their axonal compartments (Chang *et al.* 1983; Smith *et al.* 1990; Shink *et al.* 1996; Bevan *et al.* 1997). Thus in order to determine whether somatodendritic rather than axonal $GABA_A$ receptors regulate firing in STN neurons, the magnitude of $GABA_A$ receptor-mediated hyperpolarization and outward currents evoked by compartment-selective applications of GABA in the presence of the $GABA_B$ receptor antagonist CGP 55845 (2 μM) were compared. In individual neurons (Fig. 9*A–D*) and across the sample population, we found that somatodendritic applications of GABA generated greater hyperpolarization than axonal applications (peak amplitude of GABA-evoked potential; somata/dendrites = 15.5 ± 7.8 mV, $n = 7$ sites; axons = 6.6 ± 4.0 mV, $n = 8$ sites, $P = 0.009$, Mann–Whitney U test). Similarly the peak amplitude of GABA-evoked outward current was greater for somatic and dendritic than axonal application (dendrites = 79.2 ± 29.1 pA, $n = 6$; somata = 85.3 ± 38.3 pA, $n = 5$; axons = 22.5 ± 22.5 pA, $n = 17$; ANOVA, $P < 0.0001$; Bonferroni's multiple comparison test: dendrites *versus* somata, not significant (n.s.); dendrites *versus* axons, $P < 0.05$; somata *versus* axons, $P < 0.05$). Smaller outward currents seen with applications to proximal axonal sites may reflect diffusion to somatodendritic $GABA_A$ receptors because the maximal rate of increase of GABA-evoked current was relatively small compared to currents evoked by somatodendritic application (maximal rate of increase of GABA-evoked current; dendrites = 10.3 ± 3.5 pA m s^{-1}, $n = 6$; somata = 7.1 ± 5.5 pA m s^{-1}, $n = 5$; axons = 1.5 ± 1.3 pA m s^{-1}, $n = 17$; ANOVA $P < 0.0001$; Bonferroni's multiple comparison test: dendrites *versus* somata, n.s.; dendrites *versus* axons $P < 0.05$; somata *versus* axons, $P < 0.05$).

Because poor voltage control may confound the measurements described above (Williams & Mitchell, 2008), the axon initial segments of the two Golgi-labelled neurons illustrated in Fig. 3 were examined in their entirety through electron microscopic examination of serial ultrathin sections in order to more definitively determine whether this compartment receives synaptic input. Synaptic terminals with the morphological properties of GABAergic globus pallidus terminals (Smith *et al.* 1990; Bevan *et al.* 1997) were readily identified in synaptic contact with the dendrites and somata/axon hillock of each STN neuron (Fig. 10). In contrast, synaptic inputs to the axon initial segment > 2–3 μm from the soma were not observed (Fig. 11). Taken together with earlier studies (Bevan *et al.* 2002; Baufreton *et al.* 2005; Hallworth & Bevan, 2005), these data suggest that the synaptic activation of somatodendritic $GABA_A$ receptors tightly regulates action potential generation in STN neurons through actions on Na_v channels in proximal axonal and somatic compartments.

Discussion

Loose-seal cell-attached recording of action potential initiation and propagation

Visually guided loose-seal cell-attached recordings have recently been used to record action potentials in small diameter neuronal compartments (Clark *et al.* 2005; Khaliq & Raman, 2005, 2006; Meeks *et al.* 2005; Monsivais *et al.* 2005; Meeks & Mennerick, 2007). Several lines of evidence reported here and in recent studies demonstrate that this signal is related to the local capacitive voltage transient associated with an action potential: (1) extracellular recordings close to the compartment of interest, in contrast to loose-seal cell-attached recordings, are associated with relatively small signals of variable polarity (Meeks *et al.* 2005; Teagarden *et al.* 2008); (2) simultaneous whole-cell and loose-seal cell-attached recordings from the same neuronal compartment have confirmed that the loose-seal measurement is similar in form to the first temporal derivative of the whole-cell record (Meeks *et al.* 2005; Teagarden *et al.* 2008); (3) conduction velocity estimates based on loose-seal cell-attached recording are in accord with estimates based on electrical axonal/synaptic stimulation experiments *in vitro* and *in vivo* (Khaliq & Raman, 2005; Meeks *et al.* 2005; Meeks & Mennerick, 2007; Teagarden *et al.* 2008).

Site of initiation of autonomously generated action potentials

Simultaneous whole-cell somatic and loose-seal cell-attached recordings demonstrated that action potentials were initiated in the proximal axon of STN neurons. These findings are consistent with findings from the hippocampus (Meeks & Mennerick, 2007; Schmidt-Hieber *et al.* 2008), neocortex (Kole *et al.* 2007; Shu *et al.* 2007) and cerebellum (Clark *et al.* 2005). In both neurons with myelinated or unmyelinated axons, loose-seal cell-attached and whole-cell recordings have demonstrated that action potentials are typically initiated in the proximal axon. As in our study, these estimates have arisen from the composition of data arising from multiple neurons in which few sites were sampled. Simultaneous sampling of action potential generation in multiple compartments of individual neurons has also

been achieved through voltage-sensitive dye imaging (Palmer & Stuart, 2006) in a study, which also suggested initiation in the proximal axon. The precise site of initiation in the proximal axon does, however, appear to vary. In Purkinje neurons, initiation occurs at the first node of Ranvier ∼80 μm from the soma (Clark *et al.* 2005). In CA3 hippocampal pyramidal neurons (which are unmyelinated up to 1 mm from the soma) the data suggest a zone of initiation in the axon 10–100 μm from the soma (Meeks & Mennerick, 2007). In somatosensory cortical pyramidal neurons initiation occurs in the distal non-myelinated axon initial segment ∼35 μm from the soma (Palmer & Stuart, 2006; Kole *et al.* 2007). In prefrontal cortical pyramidal neurons (which become myelinated several hundred micrometres from the soma) initiation occurs in the proximal axon within 30–45 μm from the soma (Shu *et al.* 2007). Finally, in non-myelinated hippocampal granule cells initiation occurs in the axon 20–30 μm from the soma (Schmidt-Hieber *et al.* 2008). Our measurements first detected action potentials in a region that most closely corresponded to the axon initial segment. Simultaneous sampling of voltage in multiple compartments of individual STN neurons will, however, be required for a definitive determination of the site of initiation.

Axonal and dendritic propagation of autonomously generated action potentials

Propagation of action potentials may fail due to the level and pattern of expression of Na_v and other channel

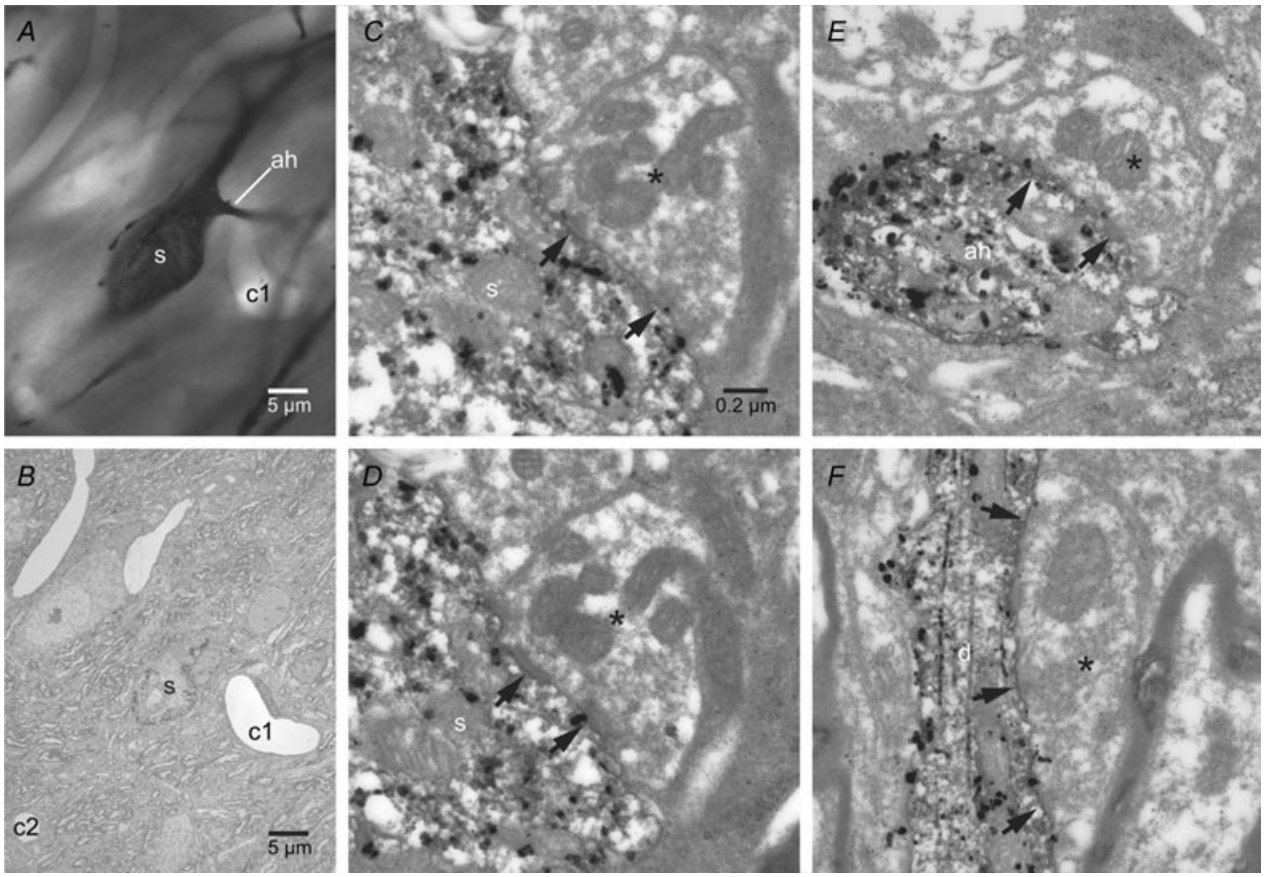

Figure 10. The soma, axon hillock and dendrites of Golgi-labelled STN neurons receive synaptic inputs from putative globus pallidus terminals
A–E, light (*A*) and electron (*B–F*) micrographs of the soma (s) and axon hillock (ah) of a Golgi-labelled neuron (the distal axon of this neuron is also illustrated in Figs 3*B* and 11). A capillary (c1) acts as a point of registration between the light and electron micrographs. *C–E*, the soma (*C* and *D*) and axon hillock (*E*) of this neuron received synaptic input (arrows) from terminals (asterisks) that possessed the morphological properties of terminals arising from GABAergic globus pallidus neurons, i.e. they were large, formed multiple symmetrical synaptic junctions and contained multiple mitochondria. *C* and *D*, serial sections through the same axosomatic terminal. *E*, the axo-axonic synapse was established on the axon hillock ∼2–3 μm from the soma. *F*, an example of another globus pallidus-like terminal (asterisk) that formed multiple symmetrical synaptic contacts (arrows) with the dendrite (d) of another Golgi-labelled STN neuron. Scale bar in *C* also applies to *D–F*.

subtypes in specific compartments (Spruston *et al.* 1995; Debanne *et al.* 1997; Jung *et al.* 1997; Debanne, 2004; Gentet & Williams, 2007) and at the interface of the axon and soma and at axonal and dendritic branch points due to the capacitive load of these junctions (Grossman *et al.* 1979; Debanne, 2004). In midbrain dopamine neurons for example, action potentials often fail to generate a full somatic action potential (Grace & Bunney, 1983; Gentet & Williams, 2007). Action potentials can also exhibit frequency-dependent failures of propagation due in some cases to inactivation of Na_v channels (Coombs *et al.* 1957; Fuortes *et al.* 1957; Grace & Bunney, 1983; Spruston *et al.*

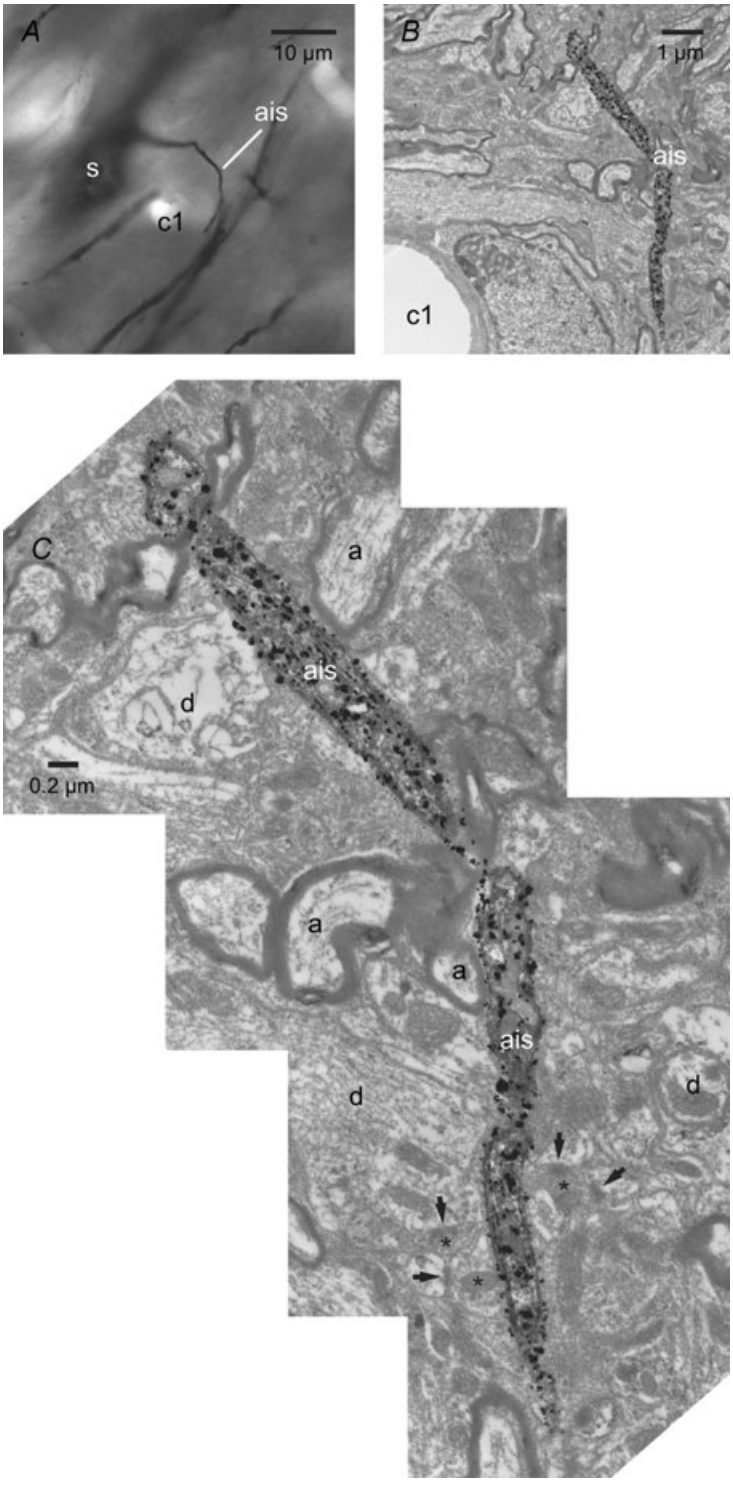

Figure 11. The axon initial segment is largely devoid of synaptic input
A–C, light (*A*) and electron (*B* and *C*) micrographs of the axon initial segment (ais) of the Golgi-labelled neuron illustrated in Figs 3*B* and 10*A–E*. The capillary (c1) acts as a point of registration between the light and electron micrographs. Although the axon hillock received an input from a putative globus pallidus terminal (Fig. 10*E*), the remaining axon initial segment did not receive synaptic input. At high magnification (*C*), the axon can be observed to course through neuropil in which adjacent axons (a), dendrites (d), synaptic terminals (asterisks) and synapses (arrows) with other elements are present.

1995; Jung *et al.* 1997; Do & Bean, 2003; Debanne, 2004; Khaliq & Raman, 2005; Meeks *et al.* 2005; Monsivais *et al.* 2005; Scott *et al.* 2007; Shu *et al.* 2007). However, action potentials in the proximal axon of STN neurons always led to full amplitude somatic action potentials and propagated reliably into distal axons and dendrites (often beyond branch points). These data are therefore in accord with the consistency of action potential-associated dendritic Ca^{2+} transients in STN neurons (Teagarden *et al.* 2008) and the role of STN neurons as a tonic 'driving force' *in vivo* (Tachibana *et al.* 2008).

As expected, the conduction velocity of the myelinated axon was considerably faster than the velocity of action potentials in the dendritic compartment of STN neurons. The axonal conduction velocity estimate was also consistent with conduction velocities estimated from axonal and synaptic stimulation studies *in vitro* and *in vivo* (Kita *et al.* 1983*a*; Nakanishi *et al.* 1987*b*, 1991; Granata & Kitai, 1989; Kita & Kitai, 1991). Linear fits to the relationship between the timing of action potentials and distance of measurement in each compartment were, however, poorer for the myelinated axon than for the dendritic compartment. This could reflect underlying heterogeneity in the conduction velocity of STN axons (Kita *et al.* 1983*a*; Nakanishi *et al.* 1987*b*, 1991; Granata & Kitai, 1989; Kita & Kitai, 1991). The distance of recordings from nodes of Ranvier will also affect the apparent conduction velocity because internodal recordings will measure the axial propagation of action potentials from adjacent nodes that are proximal and/or distal to the soma (Clark *et al.* 2005; Palmer & Stuart, 2006; Kole *et al.* 2008).

The location of Na_v channels responsible for the autonomous initiation of action potentials

We found that variable transection of STN axons did not significantly alter the shape, threshold or maximum rate of rise of action potentials recorded at the soma. Similar findings have been reported for cortical pyramidal neurons (Palmer & Stuart, 2006). The failure of axonal transections beyond or within the axon initial segment to affect action potential formation suggests that neurons express a large reserve of Na_v channels (Madeja, 2000) within the axon initial segment and soma for action potential generation. Indeed, autonomous activity of STN neurons persists despite inactivation of ~40% of Na_v channels (Do & Bean, 2003; Baufreton *et al.* 2005). These data also confirm that Na_v channels in nodes of Ranvier beyond the axon initial segment are not necessary for autonomous firing in STN neurons.

2PLSM-guided application of low $[Na^+]$ ACSF or TTX revealed that manipulation of Na_v channels in the axon initial segment most consistently elevated threshold, whereas applications at more distal axonal sites or the soma itself elevated threshold in a subset of neurons. Whether these observations reflect underlying heterogeneity in the distribution of Na_v channels (Kuba *et al.* 2006), or diffusion to axon initial segment Na_v channels is unknown. Applications centred on dendrites were without effect. Together these data suggest that Na_v channels in the axon initial segment are most critical for the initiation of action potentials in STN neurons, a conclusion that is consistent with the earliest detection of action potentials in a similar region. The capability of low $[Na^+]$ ACSF or TTX application rather than physical removal of axonal Na_v channels to detect changes in action potential properties is likely to reflect the enhanced sensitivity of the within-cell design of the application experiments. Our findings are also consistent with the effects of similar application experiments in most neurons studied thus far (Khaliq & Raman, 2006; Palmer & Stuart, 2006; Meeks & Mennerick, 2007). However, in subicular pyramidal neurons nodal Na_v channels appear critical for action potential generation because threshold was only elevated by TTX application beyond the initial segment (Colbert & Johnston, 1996).

Location of GABA receptors

Recent studies have suggested that $GABA_A$ receptor-mediated inputs regulate the pattern of STN neuronal activity in part through their effects on postsynaptic Na_v channels (Bevan *et al.* 2002; Baufreton *et al.* 2005). In some neurons, the availability and state of axonal Na_v channels are regulated directly by axo-axonic GABAergic inputs. However, earlier ultrastructural studies have suggested that GABAergic inputs are directed to the somatodendritic compartment of STN neurons with occasional inputs to the axon hillock (Chang *et al.* 1983; Smith *et al.* 1990; Shink *et al.* 1996; Bevan *et al.* 1997). Given the difficulty in recognizing the unlabelled axon initial segment and the fact that extrasynaptic $GABA_A$ receptors can be activated by spillover from GABA synapses (Kullmann, 2000; Farrant & Nusser, 2005), local applications of GABA were used as a probe for functional $GABA_A$ receptors. Although small $GABA_A$ receptor-mediated currents were generated by axonal applications of GABA, their small amplitude and slow kinetics, compared to currents evoked by somatic or dendritic applications suggest that axonally applied GABA diffused to and activated somatodendritic $GABA_A$ receptors. Electron microscopic analysis of serial ultrathin sections through two Golgi-labelled STN neurons confirmed that, in contrast to somatic and dendritic compartments, the axon initial segment of STN neurons was indeed largely devoid of synaptic input from putative GABAergic terminals.

Functional implications

Theoretical studies suggest that the placement of Na_v channels in the proximal axon represents an efficient strategy for action potential formation given the low effective capacitance of this small diameter compartment compared to the soma and dendritic arbor (Mainen *et al.* 1995; Colbert & Pan, 2002; Clark *et al.* 2005; Meeks & Mennerick, 2007; Mercer *et al.* 2007; Kole *et al.* 2008; Schmidt-Hieber *et al.* 2008). In myelinated axons the proximity of this compartment to myelin additionally aids action potential formation by further lowering local capacitance (Mainen *et al.* 1995; Colbert & Pan, 2002; Clark *et al.* 2005; Meeks & Mennerick, 2007; Mercer *et al.* 2007; Kole *et al.* 2008; Schmidt-Hieber *et al.* 2008). These strategies, which are highly conserved, will therefore minimize the number of Na_v channels required for action potential generation. In STN neurons the proximity of the axonal site of initiation to somatodendritic synaptic inputs (Chang *et al.* 1983; Smith *et al.* 1990; Bevan *et al.* 1995, 1997; Shink *et al.* 1996) will therefore enable synaptic inputs to regulate proximal axonal Na_v channels through effects on axonal voltage without directly affecting the resistance of the axolemma. Indeed, recent studies suggest that inhibitory and excitatory postsynaptic potentials arising from inputs to the somatodendritic compartment can effectively regulate the voltage of axons and synaptic terminals even at sites considerably distal to the site of initiation (Alle & Geiger, 2006; Shu *et al.* 2006; Kole *et al.* 2007).

In most neurons and under most conditions studied thus far synaptic inputs do not shift the site of initiation of action potentials to the soma or dendrites although dendritic Na_v and Ca_v channels may contribute to local regenerative potentials that play a role in the integration of synaptic inputs (Magee, 2000; Gulledge *et al.* 2005; London & Häusser, 2005; Losonczy & Magee, 2006; Spruston, 2008). If a similar principle holds true for STN neurons then synaptic inputs to their somata and dendrites will regulate neuronal output via a common region of action potential initiation in the proximal axon. Manipulations that interfere with the synaptic patterning of action potential generation in the proximal axon could therefore be of therapeutic value in correcting the pathological output of the STN in PD. Indeed, an interesting hypothesis for the therapeutic effect of high-frequency electrical stimulation of the STN for PD is that stimulation silences the normal site of initiation through activation of GABAergic inputs and simultaneously entrains action potential generation in the distal axon of STN neurons (McIntyre *et al.* 2004). The application of simultaneous whole-cell somatic and axonal loose-seal cell-attached recordings during high-frequency electrical stimulation of the STN will enable a direct test of this hypothesis.

References

Afsharpour S (1985). Light microscopic analysis of Golgi-impregnated rat subthalamic neurons. *J Comp Neurol* **236**, 1–13.

Albin RL, Young AB & Penney JB (1989). The functional anatomy of basal ganglia disorders. *Trends Neurosci* **12**, 366–375.

Alle H & Geiger JR (2006). Combined analog and action potential coding in hippocampal mossy fibers. *Science* **311**, 1290–1293.

Alvarez L, Macias R, Lopez G, Alvarez E, Pavon N, Rodriguez-Oroz MC, Juncos JL, Maragoto C, Guridi J, Litvan I, Tolosa ES, Koller W, Vitek J, DeLong MR & Obeso JA (2005). Bilateral subthalamotomy in Parkinson's disease: initial and long-term response. *Brain* **128**, 570–583.

Astman N, Gutnick MJ & Fleidervish IA (2006). Persistent sodium current in layer 5 neocortical neurons is primarily generated in the proximal axon. *J Neurosci* **26**, 3465–3473.

Bar-Gad I, Morris G & Bergman H (2003). Information processing, dimensionality reduction and reinforcement learning in the basal ganglia. *Prog Neurobiol* **71**, 439–473.

Baufreton J, Atherton JF, Surmeier DJ & Bevan MD (2005). Enhancement of excitatory synaptic integration by GABAergic inhibition in the subthalamic nucleus. *J Neurosci* **25**, 8505–8517.

Benabid AL (2003). Deep brain stimulation for Parkinson's disease. *Curr Opin Neurobiol* **13**, 696–706.

Bennett V & Lambert S (1999). Physiological roles of axonal ankyrins in survival of premyelinated axons and localization of voltage-gated sodium channels. *J Neurocytol* **28**, 303–318.

Bergman H, Wichmann T & DeLong MR (1990). Reversal of experimental parkinsonism by lesions of the subthalamic nucleus. *Science* **249**, 1436–1438.

Bergman H, Wichmann T, Karmon B & DeLong MR (1994). The primate subthalamic nucleus. II. Neuronal activity in the MPTP model of parkinsonism. *J Neurophysiol* **72**, 507–520.

Beurrier C, Bioulac B & Hammond C (2000). Slowly inactivating sodium current (I_{NaP}) underlies single-spike activity in rat subthalamic neurons. *J Neurophysiol* **83**, 1951–1957.

Beurrier C, Congar P, Bioulac B & Hammond C (1999). Subthalamic nucleus neurons switch from single-spike activity to burst-firing mode. *J Neurosci* **19**, 599–609.

Bevan MD, Clarke NP & Bolam JP (1997). Synaptic integration of functionally diverse pallidal information in the entopeduncular nucleus and subthalamic nucleus in the rat. *J Neurosci* **17**, 308–324.

Bevan MD, Francis CM & Bolam JP (1995). The glutamate-enriched cortical and thalamic input to neurons in the subthalamic nucleus of the rat: convergence with GABA-positive terminals. *J Comp Neurol* **361**, 491–511.

Bevan MD, Magill PJ, Hallworth NE, Bolam JP & Wilson CJ (2002). Regulation of the timing and pattern of action potential generation in rat subthalamic neurons in vitro by GABA-A IPSPs. *J Neurophysiol* **87**, 1348–1362.

Bevan MD & Wilson CJ (1999). Mechanisms underlying spontaneous oscillation and rhythmic firing in rat subthalamic neurons. *J Neurosci* **19**, 7617–7628.

Brown P, Oliviero A, Mazzone P, Insola A, Tonali P & Di Lazzaro V (2001). Dopamine dependency of oscillations between subthalamic nucleus and pallidum in Parkinson's disease. *J Neurosci* **21**, 1033–1038.

Buhl EH, Cobb SR, Halasy K & Somogyi P (1995). Properties of unitary IPSPs evoked by anatomically identified basket cells in the rat hippocampus. *Eur J Neurosci* **7**, 1989–2004.

Castelli L, Biella G, Toselli M & Magistretti J (2007). Resurgent Na^+ current in pyramidal neurones of rat perirhinal cortex: axonal location of channels and contribution to depolarizing drive during repetitive firing. *J Physiol* **582**, 1179–1193.

Chang HT, Kita H & Kitai ST (1983). The fine structure of the rat subthalamic nucleus: an electron microscopic study. *J Comp Neurol* **221**, 113–123.

Clark BA, Monsivais P, Branco T, London M & Häusser M (2005). The site of action potential initiation in cerebellar Purkinje neurons. *Nat Neurosci* **8**, 137–139.

Colbert CM & Johnston D (1996). Axonal action-potential initiation and Na^+ channel densities in the soma and axon initial segment of subicular pyramidal neurons. *J Neurosci* **16**, 6676–6686.

Colbert CM & Pan E (2002). Ion channel properties underlying axonal action potential initiation in pyramidal neurons. *Nat Neurosci* **5**, 533–538.

Coombs JS, Curtis DR & Eccles JC (1957). The interpretation of spike potentials of motoneurones. *J Physiol* **139**, 198–231.

Crossman AR (1989). Neural mechanisms in disorders of movement. *Comp Biochem Physiol A* **93**, 141–149.

Debanne D (2004). Information processing in the axon. *Nat Rev Neurosci* **5**, 304–316.

Debanne D, Guerineau NC, Gahwiler BH & Thompson SM (1997). Action-potential propagation gated by an axonal I_A-like K^+ conductance in hippocampus. *Nature* **389**, 286–289.

DeLong MR (1990). Primate models of movement disorders of basal ganglia origin. *Trends Neurosci* **13**, 281–285.

DeLong MR, Alexander GE, Mitchell SJ & Richardson RT (1986). The contribution of basal ganglia to limb control. *Prog Brain Res* **64**, 161–174.

Do MT & Bean BP (2003). Subthreshold sodium currents and pacemaking of subthalamic neurons: modulation by slow inactivation. *Neuron* **39**, 109–120.

Fairen A, Peters A & Saldanha J (1977). A new procedure for examining Golgi impregnated neurons by light and electron microscopy. *J Neurocytol* **6**, 311–337.

Farrant M & Nusser Z (2005). Variations on an inhibitory theme: phasic and tonic activation of $GABA_A$ receptors. *Nat Rev Neurosci* **6**, 215–229.

Fuortes MGF, Frank K & Becker MC (1957). Steps in the production of motoneuron spikes. *J Gen Physiol* **40**, 735–752.

Gabbott PL & Somogyi J (1984). The 'single' section Golgi-impregnation procedure: methodological description. *J Neurosci Methods* **11**, 221–230.

Gentet LJ & Williams SR (2007). Dopamine gates action potential backpropagation in midbrain dopaminergic neurons. *J Neurosci* **27**, 1892–1901.

Grace AA & Bunney BS (1983). Intracellular and extracellular electrophysiology of nigral dopaminergic neurons – 2. Action potential generating mechanisms and morphological correlates. *Neuroscience* **10**, 317–331.

Granata AR & Kitai ST (1989). Intracellular analysis of excitatory subthalamic inputs to the pedunculopontine neurons. *Brain Res* **488**, 57–72.

Graybiel AM, Aosaki T, Flaherty AW & Kimura M (1994). The basal ganglia and adaptive motor control. *Science* **265**, 1826–1831.

Grossman Y, Parnas I & Spira ME (1979). Differential conduction block in branches of a bifurcating axon. *J Physiol* **295**, 283–305.

Gulledge AT, Kampa BM & Stuart GJ (2005). Synaptic integration in dendritic trees. *J Neurobiol* **64**, 75–90.

Hallworth NE & Bevan MD (2005). Globus pallidus neurons dynamically regulate the activity pattern of subthalamic nucleus neurons through the frequency-dependent activation of postsynaptic $GABA_A$ and $GABA_B$ receptors. *J Neurosci* **25**, 6304–6315.

Hallworth NE, Wilson CJ & Bevan MD (2003). Apamin-sensitive small conductance calcium-activated potassium channels, through their selective coupling to voltage-gated calcium channels, are critical determinants of the precision, pace, and pattern of action potential generation in rat subthalamic nucleus neurons in vitro. *J Neurosci* **23**, 7525–7542.

Hamani C, Neimat J & Lozano AM (2006). Deep brain stimulation for the treatment of Parkinson's disease. *J Neural Transm Suppl*, 393–399.

Häusser M & Clark BA (1997). Tonic synaptic inhibition modulates neuronal output pattern and spatiotemporal synaptic integration. *Neuron* **19**, 665–678.

Häusser M, Stuart G, Racca C & Sakmann B (1995). Axonal initiation and active dendritic propagation of action potentials in substantia nigra neurons. *Neuron* **15**, 637–647.

Hikosaka O, Nakamura K & Nakahara H (2006). Basal ganglia orient eyes to reward. *J Neurophysiol* **95**, 567–584.

Jung HY, Mickus T & Spruston N (1997). Prolonged sodium channel inactivation contributes to dendritic action potential attenuation in hippocampal pyramidal neurons. *J Neurosci* **17**, 6639–6646.

Khaliq ZM, Gouwens NW & Raman IM (2003). The contribution of resurgent sodium current to high-frequency firing in Purkinje neurons: an experimental and modeling study. *J Neurosci* **23**, 4899–4912.

Khaliq ZM & Raman IM (2005). Axonal propagation of simple and complex spikes in cerebellar Purkinje neurons. *J Neurosci* **25**, 454–463.

Khaliq ZM & Raman IM (2006). Relative contributions of axonal and somatic Na channels to action potential initiation in cerebellar Purkinje neurons. *J Neurosci* **26**, 1935–1944.

Kita H, Chang HT & Kitai ST (1983*a*). Pallidal inputs to subthalamus: intracellular analysis. *Brain Res* **264**, 255–265.

Kita H, Chang HT & Kitai ST (1983*b*). The morphology of intracellularly labeled rat subthalamic neurons: a light microscopic analysis. *J Comp Neurol* **215**, 245–257.

Kita H & Kitai ST (1991). Intracellular study of rat globus pallidus neurons: membrane properties and responses to neostriatal, subthalamic and nigral stimulation. *Brain Res* **564**, 296–305.

Kole MH, Ilschner SU, Kampa BM, Williams SR, Ruben PC & Stuart GJ (2008). Action potential generation requires a high sodium channel density in the axon initial segment. *Nat Neurosci* **11**, 178–186.

Kole MH, Letzkus JJ & Stuart GJ (2007). Axon initial segment Kv1 channels control axonal action potential waveform and synaptic efficacy. *Neuron* **55**, 633–647.

Kuba H, Ishii TM & Ohmori H (2006). Axonal site of spike initiation enhances auditory coincidence detection. *Nature* **444**, 1069–1072.

Kullmann DM (2000). Spillover and synaptic cross talk mediated by glutamate and GABA in the mammalian brain. *Prog Brain Res* **125**, 339–351.

Levy R, Ashby P, Hutchison WD, Lang AE, Lozano AM & Dostrovsky JO (2002). Dependence of subthalamic nucleus oscillations on movement and dopamine in Parkinson's disease. *Brain* **125**, 1196–1209.

Levy R, Dostrovsky JO, Lang AE, Sime E, Hutchison WD & Lozano AM (2001). Effects of apomorphine on subthalamic nucleus and globus pallidus internus neurons in patients with Parkinson's disease. *J Neurophysiol* **86**, 249–260.

Levy R, Hutchison WD, Lozano AM & Dostrovsky JO (2000). High-frequency synchronization of neuronal activity in the subthalamic nucleus of parkinsonian patients with limb tremor. *J Neurosci* **20**, 7766–7775.

London M & Häusser M (2005). Dendritic computation. *Annu Rev Neurosci* **28**, 503–532.

Losonczy A & Magee JC (2006). Integrative properties of radial oblique dendrites in hippocampal CA1 pyramidal neurons. *Neuron* **50**, 291–307.

McIntyre CC, Savasta M, Kerkerian-Le Goff L & Vitek JL (2004). Uncovering the mechanism(s) of action of deep brain stimulation: activation, inhibition, or both. *Clin Neurophysiol* **115**, 1239–1248.

Madeja M (2000). Do neurons have a reserve of sodium channels for the generation of action potentials? A study on acutely isolated CA1 neurons from the guinea-pig hippocampus. *Eur J Neurosci* **12**, 1–7.

Magee JC (2000). Dendritic integration of excitatory synaptic input. *Nat Rev Neurosci* **1**, 181–190.

Mainen ZF, Joerges J, Huguenard JR & Sejnowski TJ (1995). A model of spike initiation in neocortical pyramidal neurons. *Neuron* **15**, 1427–1439.

Meeks JP, Jiang X & Mennerick S (2005). Action potential fidelity during normal and epileptiform activity in paired soma-axon recordings from rat hippocampus. *J Physiol* **566**, 425–441.

Meeks JP & Mennerick S (2007). Action potential initiation and propagation in CA3 pyramidal axons. *J Neurophysiol* **97**, 3460–3472.

Mercer JN, Chan CS, Tkatch T, Held J & Surmeier DJ (2007). Nav1.6 sodium channels are critical to pacemaking and fast spiking in globus pallidus neurons. *J Neurosci* **27**, 13552–13566.

Miles R, Toth K, Gulyas AI, Hajos N & Freund TF (1996). Differences between somatic and dendritic inhibition in the hippocampus. *Neuron* **16**, 815–823.

Mink JW & Thach WT (1993). Basal ganglia intrinsic circuits and their role in behavior. *Curr Opin Neurobiol* **3**, 950–957.

Monsivais P, Clark BA, Roth A & Häusser M (2005). Determinants of action potential propagation in cerebellar Purkinje cell axons. *J Neurosci* **25**, 464–472.

Nakanishi H, Kita H & Kitai ST (1987*a*). Electrical membrane properties of rat subthalamic neurons in an in vitro slice preparation. *Brain Res* **437**, 35–44.

Nakanishi H, Kita H & Kitai ST (1987*b*). Intracellular study of rat substantia nigra pars reticulata neurons in an in vitro slice preparation: electrical membrane properties and response characteristics to subthalamic stimulation. *Brain Res* **437**, 45–55.

Nakanishi H, Kita H & Kitai ST (1991). Intracellular study of rat entopeduncular nucleus neurons in an in vitro slice preparation: response to subthalamic stimulation. *Brain Res* **549**, 285–291.

Overton PG & Greenfield SA (1995). Determinants of neuronal firing pattern in the guinea-pig subthalamic nucleus: an in vivo and in vitro comparison. *J Neural Transm Park Dis Dement Sect* **10**, 41–54.

Palmer LM & Stuart GJ (2006). Site of action potential initiation in layer 5 pyramidal neurons. *J Neurosci* **26**, 1854–1863.

Person AL & Perkel DJ (2005). Unitary IPSPs drive precise thalamic spiking in a circuit required for learning. *Neuron* **46**, 129–140.

Peters A (2007). Golgi, Cajal, and the fine structure of the nervous system. *Brain Res Rev* **55**, 256–263.

Pouzat C & Hestrin S (1997). Developmental regulation of basket/stellate cell→Purkinje cell synapses in the cerebellum. *J Neurosci* **17**, 9104–9112.

Raman IM & Bean BP (1999). Ionic currents underlying spontaneous action potentials in isolated cerebellar Purkinje neurons. *J Neurosci* **19**, 1663–1674.

Sanchez-Vives MV & McCormick DA (2000). Cellular and network mechanisms of rhythmic recurrent activity in neocortex. *Nat Neurosci* **3**, 1027–1034.

Schmidt-Hieber C, Jonas P & Bischofberger J (2008). Action potential initiation and propagation in hippocampal mossy fibre axons. *J Physiol* **586**, 1849–1857.

Scott LL, Hage TA & Golding NL (2007). Weak action potential backpropagation is associated with high-frequency axonal firing capability in principal neurons of the gerbil medial superior olive. *J Physiol* **583**, 647–661.

Shink E, Bevan MD, Bolam JP & Smith Y (1996). The subthalamic nucleus and the external pallidum: two tightly interconnected structures that control the output of the basal ganglia in the monkey. *Neuroscience* **73**, 335–357.

Shu Y, Duque A, Yu Y, Haider B & McCormick DA (2007). Properties of action-potential initiation in neocortical pyramidal cells: evidence from whole cell axon recordings. *J Neurophysiol* **97**, 746–760.

Shu Y, Hasenstaub A, Duque A, Yu Y & McCormick DA (2006). Modulation of intracortical synaptic potentials by presynaptic somatic membrane potential. *Nature* **441**, 761–765.

Smith Y, Bolam JP & Von Krosigk M (1990). Topographical and synaptic organization of the GABA-containing pallidosubthalamic projection in the rat. *Eur J Neurosci* **2**, 500–511.

Song WJ, Baba Y, Otsuka T & Murakami F (2000). Characterization of Ca^{2+} channels in rat subthalamic nucleus neurons. *J Neurophysiol* **84**, 2630–2637.

Spruston N (2008). Pyramidal neurons: dendritic structure and synaptic integration. *Nat Rev Neurosci* **9**, 206–221.

Spruston N, Schiller Y, Stuart G & Sakmann B (1995). Activity-dependent action potential invasion and calcium influx into hippocampal CA1 dendrites. *Science* **268**, 297–300.

Szabadics J, Varga C, Molnar G, Olah S, Barzo P & Tamas G (2006). Excitatory effect of GABAergic axo-axonic cells in cortical microcircuits. *Science* **311**, 233–235.

Tachibana Y, Kita H, Chiken S, Takada M & Nambu A (2008). Motor cortical control of internal pallidal activity through glutamatergic and GABAergic inputs in awake monkeys. *Eur J Neurosci* **27**, 238–253.

Teagarden M, Atherton JF, Bevan MD & Wilson CJ (2008). Accumulation of cytoplasmic calcium, but not apamin-sensitive afterhyperpolarization current, during high frequency firing in rat subthalamic nucleus cells. *J Physiol* **586**, 817–833.

Van Wart A, Trimmer JS & Matthews G (2007). Polarized distribution of ion channels within microdomains of the axon initial segment. *J Comp Neurol* **500**, 339–352.

Williams SR & Mitchell SJ (2008). Direct measurement of somatic voltage clamp errors in central neurons. *Nat Neurosci* **11**, 790–798.

Acknowledgements

This research was supported by the National Parkinson Foundation and NIH-NINDS Grants NS041280 and NS047085.

Supplemental material

Online supplemental material for this paper can be accessed at: http://jp.physoc.org/cgi/content/full/jphysiol.2008.155861/DC1